# CATALYTIC PRODUCTION OF LACTIC ACID FROM

# XYLOSE OVER MIXED OXIDES OF ALUMINIUM

# AND ANOTHER METAL

**Chanokporn Kosri**

**A Thesis Submitted in Partial Fulfillment of the Requirements for the**

**Degree of Master of Science in Chemistry**

**Suranaree University of Technology**

**Academic Year 2019**

# การผลิตกรดแลคติกจากไซโลส โดยการเร่งปฏิกิริยาด้วยออกไซด์ผสม
# ของอลูมิเนียมกับโลหะอื่น

นางสาวชนกภรณ์ โกศรี

วิทยานิพนธ์นี้เป็นส่วนหนึ่งของการศึกษาตามหลักสูตรปริญญาวิทยาศาสตรมหาบัณฑิต
สาขาวิชาเคมี
มหาวิทยาลัยเทคโนโลยีสุรนารี
ปีการศึกษา 2562

# CATALYTIC PRODUCTION OF LACTIC ACID FROM XYLOSE

# OVER MIXED OXIDES OF ALUMINIUM AND ANOTHER METAL

Suranaree University of Technology has approved this thesis submitted in partial fulfillment of the requirements for the Degree of Doctor of Philosophy.

Thesis Examining Committee

_____

(Prof. Dr. James R. Ketudat-Cairns)

Chairperson

_____
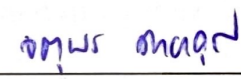
(Prof. Dr. Jatuporn Wittayakun)

Member (Thesis Advisor)

_____

(Assoc. Prof. Dr. Sanchai Prayoonpokarach)

Member

_____

(Dr. Pongnatawat Khemthong)

Member

_____  _____
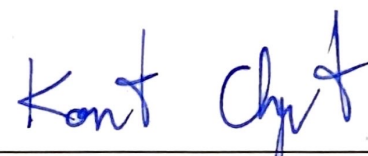
(Assoc. Prof. Flt. Lt. Dr. Kontorn Chamniprasart)  (Assoc. Prof. Dr. Worawat Meevasana)

Vice Rector for Academic Affairs  Dean of Institute of Science

and Internationalization

ชนกภรณ์ โกศรี : การผลิตกรดแลคติกจากไซโลส โดยการเร่งปฏิกิริยาด้วยออกไซด์ผสม
ของอลูมิเนียมกับโลหะอื่น (CATALYTIC PRODUCTION OF LACTIC ACID FROM
XYLOSE OVER MIXED OXIDES OF ALUMINIUM AND ANOTHER METAL)
อาจารย์ที่ปรึกษา : ศาสตราจารย์ ดร. จตุพร วิทยาคุณ, 73 หน้า.

กรดแลคติกคือสารเคมีที่สำคัญในอุตสาหกรรมหลายชนิด เช่น อาหาร ยา และเวชภัณฑ์
โดยเฉพาะอย่างยิ่งกรดพอลิแลคติก จึงมีการศึกษาการผลิตกรดแลคติกโดยการเร่งปฏิกิริยาของ
ทรัพยากรหมุนเวียน ซึ่งต้องการตัวเร่งปฏิกิริยาที่มีทั้งตำแหน่งกรดและเบส แกมมาอลูมินาเป็น
ตัวเร่งปฏิกิริยาวิวิธพันธุ์ที่มีสมบัติเป็นทั้งกรดและเบส ซึ่งมีราคาถูกและไม่มีรายงานการใช้สำหรับ
การผลิตกรดแลคติกจากไซโลส อย่างไรก็ตามผลได้ของกรดแลคติกสามารถทำให้เพิ่มขึ้นโดยการ
เพิ่มความเป็นกรดของตัวเร่ง ในงานนี้เป็นการศึกษาการเติมโลหะออกไซด์บนตัวรองรับแกมมา
อลูมินา ได้แก่ออกไซด์ของ โคบอลต์ โครเมียม ทองแดง นิกเกิล และดีบุก เพื่อเพิ่มความเป็นกรดของ
ตัวเร่งและเพิ่มผลได้ของกรดแลคติก ตัวเร่งปฏิกิริยาเตรียมโดยวิธีทำให้เอิบชุ่ม วิเคราะห์ด้วยเทคนิค
หลายชนิด เพื่อเข้าใจชนิดของโลหะออกไซด์ ลักษณะสัญฐาน พื้นที่ผิว ความเป็นกรด และความ
เป็นเบส จากนั้นนำตัวเร่งปฏิกิริยาทั้งหมดรวมถึงตัวรองรับแกมมาอลูมินาไปทดสอบการผลิตกรด
แลคติกจากไซโลส กลูโคส และกลีเซอรอล พบว่าตัวอย่างทั้งหมดมีความจำเพาะต่อการเปลี่ยน
ไซโลสเป็นกรดแลคติก ทำให้มีค่าการเปลี่ยนแปลงของไซโลสและผลได้ของกรดแลคติกสูงที่สุด
จึงใช้ไซไลสเพื่อทดสอบการผลิตกรดแลคติดโดยในเวลาที่นานขึ้น คือ 6 ชั่วโมง พบว่า ตัวเร่งที่ดี
ที่สุดคือ โครเมียมออกไซด์บนตัวรองรับแกมมาอลูมินา ซึ่งได้ถูกทดสอบเพื่อหาอุณหภูมิที่ดีที่สุดคือ
170 องศาเซลเซียส และปริมาณตัวเร่งที่เหมาะสมสำหรับการเร่งปฏิกิริยาในอุปกรณ์ทดสอบขนาด
75 มิลลิลิตร คือ 0.5 กรัม

| | |
|---|---|
| สาขาวิชาเคมี | ลายมือชื่อนักศึกษา_ชนกภรณ์ โกศรี_ |
| ปีการศึกษา 2562 | ลายมือชื่ออาจารย์ที่ปรึกษา_จตุพร วิทยาคุณ_ |

CHANOKPORN KOSRI : CATALYTIC PRODUCTION OF LACTIC ACID FROM XYLOSE OVER MIXED OXIDES OF ALUMINIUM AND ANOTHER METAL. THESIS ADVISOR : PROF. JATUPORN WITTAYAKUN, Ph.D. 73 PP.

SUPPORTED METAL OXIDE CATALYST/ GAMMA-ALUMINA/ CATALYSIS/ LACTIC ACID/ XYLOSE

Lactic acid is an important chemical in several industries such as food, pharmaceuticals, and especially polylactic acid. There are studies on lactic acid production via catalysis of renewable resources which requires catalyst with both acid and base sites. $\gamma$-$Al_2O_3$ is heterogeneous acid-base catalyst which is cheap and has not been used on lactic acid production from xylose. However, lactic acid yield can be improved by increasing the catalyst acidity. This work investigates the addition of another metal oxide on $\gamma$-$Al_2O_3$ ($M/Al_2O_3$), where M is Co, Cr, Cu, Ni, and Sn, to enhance the acidity and lactic acid formation. The catalysts were prepared by impregnation and characterized by several techniques to understand their metal oxide phase, morphology, surface area, acidity, and basicity. All catalysts and the $\gamma$-$A_2O_3$ support were tested on the transformation of xylose, glucose, and glycerol. Xylose provided highest conversion and lactic acid yield and it was tested for longer time of 6 h. The best catalyst was $Cr/Al_2O_3$. The optimal temperature was 170 °C and the suitable catalyst loading for 75 ml batch reactor was 0.5 g.

| | |
|---|---|
| School of Chemistry | Student's Signature _____ |
| Academic Year 2019 | Advisor's Signature _____ |

# ACKNOWLEDGEMENTS

# CONTENTS

# CONTENTS (Continued)

# CONTENTS (Continued)

# LIST OF TABLES

# LIST OF FIGURES

# LIST OF FIGURES (Continued)

# LIST OF FIGURES (Continued)

# CHAPTER I

# INTRODUCTION

Lactic acid ($C_3H_6O_3$) is an essential chemical in many industrial applications. It is known as an acidulant, preservative, and emulsifying agent in the food and beverage industry. Lactic acid is used as an ingredient in the production of cosmetics and pharmaceuticals, and a precursor of several value-added chemicals. Moreover, lactic acid is a monomer of polylactic acid, a biodegradable polymer (Datta and Henry, 2006).

Currently, the global production of lactic acid is mainly from bacterial fermentation of carbohydrates which are renewable resources. The main product is optically pure D- or L-lactic acid (Komesu et al., 2017). However, the major drawbacks are expensive nutrients for microbials, low volumetric productivities in upscaling, and slow process of 2-4 days (De Clercq et al., 2017). Moreover, the purification of lactic acid consists of many steps leading to generation of large amounts of wastewater and crude gypsum which require further treatment to prevent environmental problems. From these drawbacks, some researchers have used alternative strategies such as catalytic process.

The catalytic production of lactic acid involves a transformation of substrates such as carbohydrates and glycerol. The types of carbohydrates include many monosaccharides with C3 (i.e., dihydroxyacetone and glyceraldehyde), C6 (i.e., fructose and glucose), and C5 monosaccharides (De Clercq et al., 2017) have been reported. According to the literature, those monosaccharide feedstocks have similar reaction steps that involve retro-aldol condensation, isomerization, dehydration, and

intramolecular Cannizzaro reaction (Feliczak et al., 2018; Xia et al., 2018; Yang et al., 2015; Yang et al., 2016). From glycerol, the process involves dehydration and intramolecular Cannizzaro reaction (Razali and Abdullah, 2017). In this work, the substrates for lactic acid production are C5 and C6 monosaccharides (xylose and glucose, respectively) and glycerol.

The efficient catalysts in the lactic acid production, either from carbohydrates or glycerol, are acids and/or bases (Albuquerque et al., 2017; Chen et al., 2014; Tao et al., 2016; Xia et al., 2018; Yang et al., 2015). Gamma-alumina ($\gamma$-$Al_2O_3$) is a low-cost solid catalyst which has a bi-functional acid-base property. It has a high surface area and thermal stability. It is one of the most important catalysts and catalyst supports in many reactions (Euzen et al., 2002). There are reports on the use of $\gamma$-$Al_2O_3$ as a catalyst in the conversion of dihydroxyacetone to lactic acid in an aqueous solution (Takagaki et al., 2014); and dihydroxyacetone and glucose to methyl lactate in methanol solutions (Yamaguchi et al., 2018). Therefore, it is proposed in this thesis to use $\gamma$-$Al_2O_3$ as a catalyst and support in the transformation of xylose, glucose, and glycerol to lactic acid.

To improve the yield of lactic acid, the addition of metal oxides on $\gamma$-$Al_2O_3$ is considered. The yield of lactic acid is proportional to the acidity of metal oxide supported catalyst, as described by Wang et al. (2019). They have studied metal oxide-modified $Nb_2O_5$ for conversion of dihydroxylacetone to lactic acid and found that a high yield was obtained from the catalyst with the rich of acid sites. Many researchers have reported that tin chlorides ($SnCl_2$ and $SnCl_4$) (Bayu et al., 2018; Hayashi and Sasaki, 2005), copper sulfate ($CuSO_4$) (Bicker et al., 2005), cobalt sulfate ($CoSO_4$), nickel sulfate ($NiSO_4$) (Bicker et al., 2005; Kong et al., 2008), chromium chloride ($CrCl_2$ and $CrCl_3$) and chromium sulfate ($Cr_2(SO_4)_3$ (Rasrendra et al., 2011) are active

as homogeneous Lewis acid catalysts in converting biomass derived-carbohydrates to lactic acid or alkyl lactate. The homogeneous catalysts are well known to provide a fast reaction rate but they are corrosive to reactor, difficult to reuse and could contaminate the environment.

To overcome the drawbacks of homogeneous catalysts, those elements are selected in this work as solid Lewis acid sites and heterogenized by dispersing on $\gamma$-$Al_2O_3$. The combination of acid site from the metal species and $\gamma$-$Al_2O_3$ is expected to enhance xylose conversion to lactic acid. The reaction is carried out in an aqueous medium which is more environmental-friendly than organic solvents.

## References

Albuquerque, E. M., Borges, L. E. P., Fraga, M. A., and Sievers, C. (2017). Relationship between acid-base properties and the activity of $ZrO_2$-based catalysts for the Cannizzaro reaction of pyruvaldehyde to lactic acid. **ChemCatChem**. 9: 2675-2683.

Bayu, A., Yoshida, A., Karnjanakom, S., Kusakabe, K., Hao, X., Prakoso, T., Abudula, A., and Guan, G. (2018). Catalytic conversion of biomass derivatives to lactic acid with increased selectivity in an aqueous tin(II) chloride/choline chloride system. **Green Chemistry**. 20(17): 4112-4119.

Bicker, M., Endres, S., Ott, L., and Vogel, H. (2005). Catalytical conversion of carbohydrates in subcritical water: A new chemical process for lactic acid production. **Journal of Molecular Catalysis A: Chemical**. 239(1-2): 151-157.

Chen, L., Ren, S., and Ye, X. P. (2014). Lactic acid production from glycerol using CaO as solid base catalyst. **Fuel Processing Technology**. 120: 40-47.

Datta, R. and Henry, M. (2006). Lactic acid: recent advances in products, processes and technologies - a review. **Journal of Chemical Technology and Biotechnology**. 81(7): 1119-1129.

De Clercq, R., Dusselier, M., and Sels, B. F. (2017). Heterogeneous catalysis for bio-based polyester monomers from cellulosic biomass: Advances, challenges and prospects. **Green Chemistry**. 19(21): 5012-5040.

Euzen, P., Raybaud, P., Krokidis, X., Toulhoat, H., Le Loarer, J.-L., Jolivet, J.-P., and Froidefond, C. (2002). 4.7.2. Alumina. Handbook of Porous Solids, 3, Schüth, F., Sing, K.S.W., and Weitkamp, J. (eds),**Wiley-VCH Verlag GmbH, Weinheim**.

Feliczak-Guzik, A., Sprynskyy, M., Nowak, I., and Buszewski, B. (2018). Catalytic isomerization of dihydroxyacetone to lactic acid and alkyl lactates over hierarchical zeolites containing tin. **Catalysts**. 8: 31-43.

Hayashi, Y. and Sasaki, Y. (2005). Tin-catalyzed conversion of trioses to alkyl lactates in alcohol solution. **Chemical Communications**. 21: 2716-2718.

Komesu, A., Allan Rocha de Oliveira, J., Helena da Silva Martins, L., Regina Wolf Maciel, M., and Maciel Filho, R. (2017). Lactic acid manufacture. **BioResources**. 12(2): 4364-4383.

Kong, L., Li, G., Wang, H., He, W., and Ling, F. (2008). Hydrothermal catalytic conversion of biomass for lactic acid production. **Journal of Chemical Technology and Biotechnology**. 83(3): 383-388.

Rasrendra, C. B., Fachri, B. A., Makertihartha, I. G. B. N., Adisasmito, S., and Heeres, H. J. (2011). Catalytic conversion of dihydroxyacetone to lactic acid using metal salts in water. **ChemSusChem**. 4(6): 768-777.

Razali, N. and Abdullah, A. Z. (2017). Production of lactic acid from glycerol via

chemical conversion using solid catalyst: A review. **Applied Catalysis A: General**. 543: 234-246.

Takagaki, A., Jung, J. C., and Hayashi, S. (2014). Solid Lewis acidity of boehmite γ-AlO(OH) and its catalytic activity for transformation of sugars in water. **RSC Advances**. 4(82): 43785-43791.

Tao, M., Zhang, D., Deng, X., Li, X., Shi, J., and Wang, X. (2016). Lewis-acid-promoted catalytic cascade. **Chemical Communications**. 52: 3332-3335.

Wang, X., Song, Y., Huang, L., Wang, H., Huang, C., and Li, C. (2019). Tin modified $Nb_2O_5$ as an efficient solid acid catalyst for the catalytic conversion of triose sugars to lactic acid. **Catalysis Science and Technology**. 9(7): 1669-1679.

Xia, M., Dong, W., Gu, M., Chang, C., Shen, Z., and Zhang, Y. (2018). Synergetic effects of bimetals in modified beta zeolite for lactic acid synthesis from biomass-derived carbohydrates. **RSC Advances**. 8: 8965-8975.

Yamaguchi, S., Yabushita, M., Kim, M., Hirayama, J., Motokura, K., Fukuoka, A., and Nakajima, K. (2018). Catalytic conversion of biomass-derived carbohydrates to methyl lactate by acid-base bifunctional γ-$Al_2O_3$. **ACS Sustainable Chemistry and Engineering**. 6(7): 8113-8117.

Yang, L., Su, J., Carl, S., Lynam, J. G., Yang, X., and Lin, H. (2015). Catalytic conversion of hemicellulosic biomass to lactic acid in pH neutral aqueous phase media, **Applied Catalysis B : Environmental**. 162: 149-157.

Yang, L., Yang, X., Tian, E., Vattipalli, V., Fan, W., and Lin, H. (2016). Mechanistic insights into the production of methyl lactate by catalytic conversion of carbohydrates on mesoporous Zr-SBA-15. **Journal of Catalysis**. 333: 207-216.

# CHAPTER II

# LITERATURE REVIEW

This chapter provides literature review on global demand for lactic acid utilized in several applications, background of lactic acid production from bacterial fermentation and its drawback as well as lactic acid production from catalysis. Moreover, literature review of relevant catalysts for lactic acid production in this work is described.

## 2.1 Global demand for lactic acid

Lactic acid is generally used as an additive in foods and beverages, and personal care products; and as a starting material in chemical industry. Currently, lactic acid is interesting for its use in eco-friendly packaging or the biodegradable plastic industry, a growing application. Lactic acid is a monomer of polylactic acid (PLA), which is one of the most promising biodegradable polymers due to its high mechanical strength, high thermal resistance, low toxicity and biocompatibility (Gupta et al., 2007). PLA is utilized in the production of bottles, food containers, biodegradable medical devices and 3D printing fibers. The growing demand for PLA is the key to drive lactic acid production. The estimation of global lactic acid market size and value is shown in Figure 2.1. The market size is 750 kilo tons in 2014 and is expected to reach 1,844 kilo tons by 2022 with the growth rate of 12.9%. The market value is 1,275 million USD in 2014 and is expected to reach 4,129 million USD with the growth rate of 16.9% (Research and Markets, 2017).

**Figure 2.1** Global lactic acid market revenue in the year 2014-2022 (modified from https://www.researchandmarkets.com/reports/4313302/global-lactic-acid-market-size-market-share).

## 2.2 Background of lactic acid production from bacterial fermentation and its drawback

Almost all lactic acid worldwide is currently manufactured based on microbial fermentation of carbohydrates or renewable substrates. Many carbohydrate resources (e.g. molasses, corn syrup, and cane) and microbial organisms (e.g. *Lactobacillus delbrueckii*, *L. amylophilus* and *L. bulgaricus*) are used. The fermentation is generally conducted in a batch reactor and requires 2-4 days to complete. Then, optically pure D- or L-lactic acid is obtained, depending on the microbial organism used (Oliveira et al., 2018). However, nutrients are required for the organisms and excess calcium hydroxide/carbonate is added to the fermenters to neutralize the acid, maintaining the pH around 5-6. The fermented broth containing calcium lactate is separated from microbial organism, biomass, and other undesired insoluble residues to achieve purified

lactic acid. In purification, complex steps are needed to recover and purify the product from the crude fermentation broth, which include acidulation, filtration, evaporation and separation through several columns. This is a limitation for the large-scale industry because the purification process is expensive. Moreover, approximately one ton of crude gypsum, $CaSO_4$, is produced for every ton of lactic acid produced by the conventional fermentation and recovery process which needs to be disposed. Therefore the nutrient cost, separation, purification and waste treatment are drawbacks about which to be concerned (Komesu et al., 2017).

## 2.3 Background of lactic acid production from catalysis

The drawbacks in the conventional process to produce lactic acid can be reduced by using a chemical catalytic method. Several sugars in nature can be used for the production of lactic acid through the chemical catalysis process, including C3 monosaccharides (e.g. glyceraldehyde and dihydroxyacetone), C5 monosaccharides (e.g. xylose and arabinose) and C6 monosaccharides (e.g. glucose, fructose, mannose and galactose), disaccharide (e.g. sucrose), cellulose and biomass (Deng et al., 2015; Yang et al., 2015). The catalytic process could be performed in alcohol under an inert atmosphere to produce alkyl lactate or in aqueous media to produce lactic acid (Taarning et al., 2009). Many researchers have already reported the study on dihydroxyacetone (C3) and glucose (C6) as reactants, while not many have worked on xylose (C5).

The reaction steps to produce lactic acid from dihydroxyacetone or glyceraldehyde are shown in Figure 2.2. Both C3 monosaccharides can be converted to lactic acid or alkyl lactate by performing the reaction in water or alcohol, respectively. First, the

hydroxyacetone or glyceraldehyde is dehydrated to pyruvaldehyde. Meanwhile, glyceraldehyde can be rapidly isomerized to dihydroxyacetone before dehydration due to the higher thermodynamic stability of dihydroxyacetone. The pyruvaldehyde is transformed into the hydrate or hemiacetal by reaction with water or alcohol, respectively. Then, it is converted into lactic acid or alkyl lactate by a formal intramolecular Cannizzaro reaction or Meerwein-Ponndorf-Verley type reaction, which is a hydride shift between the hemiacetal carbon and the adjacent carbonyl carbon lead to more thermodynamically stable acid or ester (Ferrini et al., 2017).
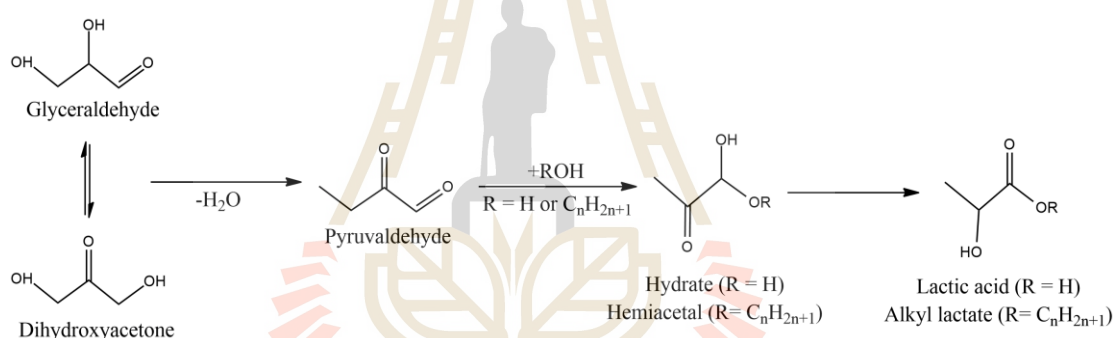
**Figure 2.2** Conversion of C3 monosaccharides to lactic acid or alkyl lactate (modified from Ferrini et al., 2017).

The reaction steps to produce lactic acid from xylose are shown in Figure 2.3. The first step is retro-aldol condensation of xylose to glycoladehyde and glyceraldehyde. The glyceraldehyde can be isomerized to dihydroxyacetone which undergoes dehydration to 2-hydroxypropenal and undergoes keto-enol tautomerization to form pyruvaldehyde. The last step is hydride transfer of pyruvaldehyde or intramolecular Cannizzaro rearrangement to lactic acid. By-products in this reaction are furfural,

glycolic acid and formic acid. Furfural is obtained from dehydration of furfural whereas glycolic acid and formic acid are obtained from oxidation of glycoladehyde.
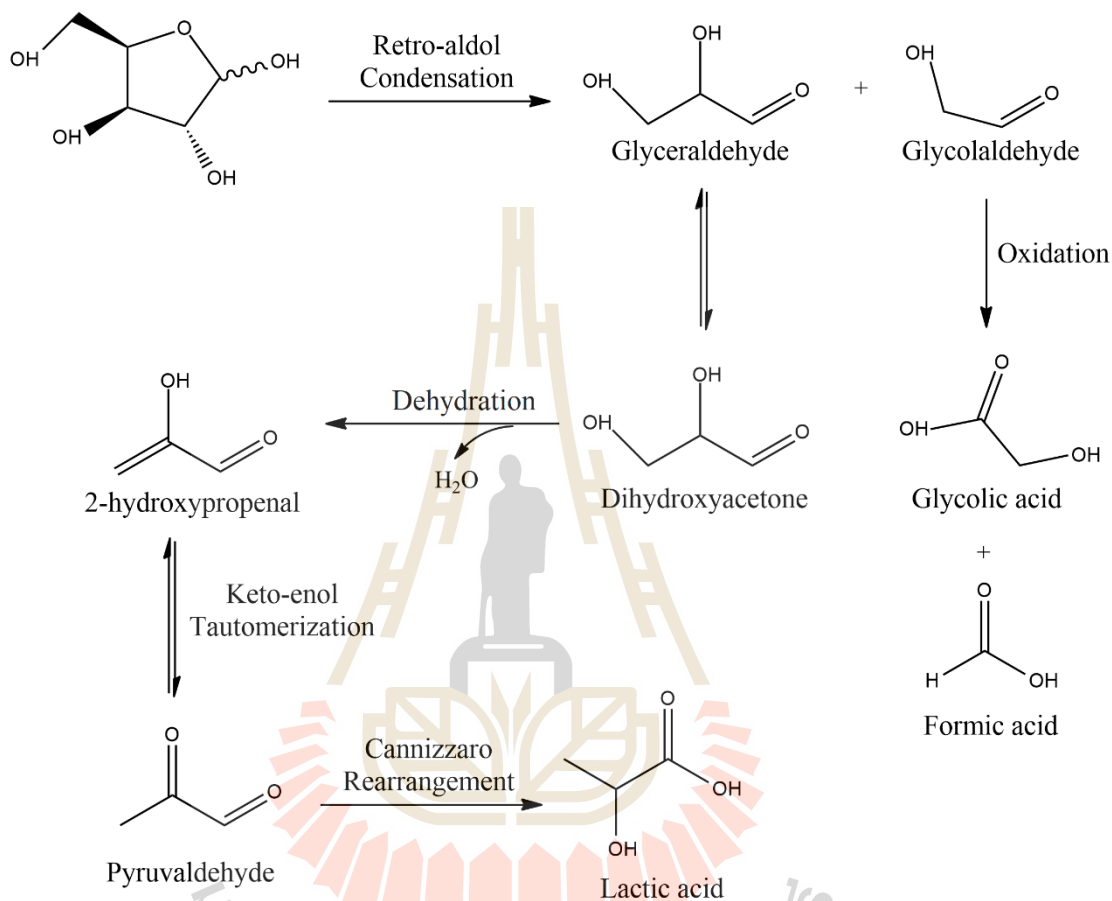


**Figure 2.3** Conversion of xylose to lactic acid (modified from Yang et al., 2015).

The reaction steps to produce lactic acid from glucose is shown in Figure 2.4. The first step is isomerization of glucose to fructose. The next step is the retro-aldol condensation of fructose to provide glyceraldehyde and dihydroxyacetone. They are important intermediates which can be dehydrated and isomerized to pyruvaldehyde. Finally, they undergo intramolecular Cannizzaro rearrangement to lactic acid. The transformations of those reactants are similar, they include retro-aldol condensation,

isomerization, dehydration and intramolecular Cannizzaro reaction (Feliczak et al., 2018; Xia et al., 2018; Yang et al., 2015; Yang et al., 2016). The retro-aldol condensation involves the cleavage of C-C bond of glucose or xylose to produce C3 intermediates which are dihydroxyacetone and glyceraldehyde. The intermediates are isomerized and dehydrated to pyruvaldehyde. Then, the intermediates undergo intramolecular Cannizzaro rearrangement to form lactic acid.
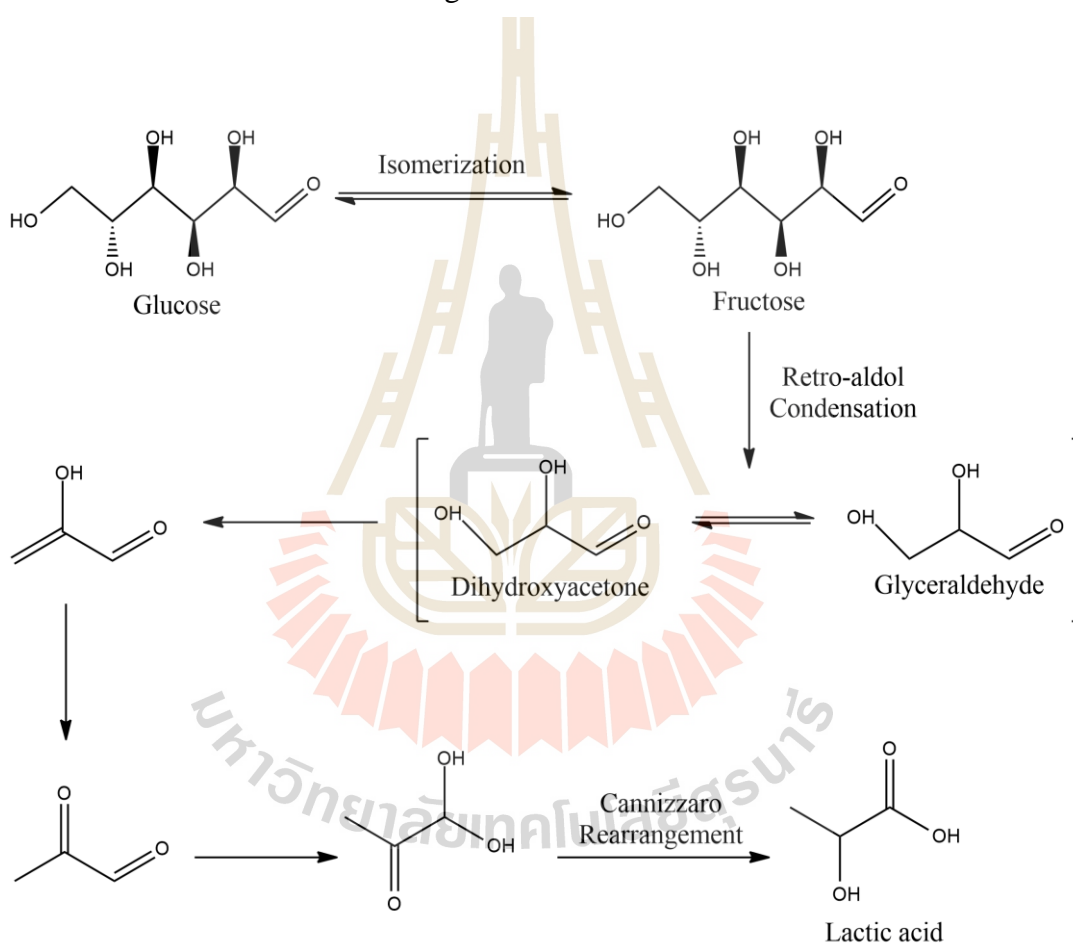


**Figure 2.4** Conversion of glucose to lactic acid (modified from Deng et al., 2018).

Moreover, glycerol, a co-product from biodiesel production, can be used as a reactant for catalytic production of lactic acid. Figure 2.5 displays reaction steps to produce lactic acid from glycerol. First, glycerol is dehydrogenated to form

glyceraldehyde as an intermediate. The next step is isomerization, dehydration and intramolecular Cannizzaro to form lactic acid. This mechanism is similar to that of monosaccharide transformation.
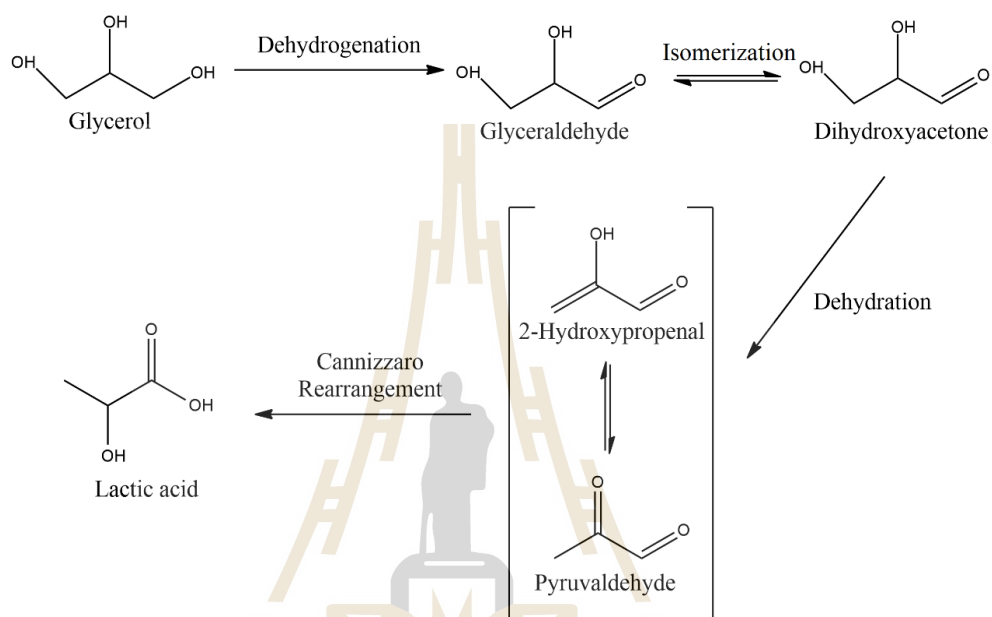


**Figure 2.5** Conversion of glycerol to lactic acid (modified from Dai et al., 2017).

## 2.4 Catalysts for lactic acid production from monosaccharides and glycerol

Lactic acid production from renewable resources has been studied on many catalysts, including homogeneous and heterogeneous ones. Many researchers have focused on the heterogeneous catalysts because they are easier to separate from reaction mixture and more environmental-friendly than the homogeneous ones. Their properties relate to the transformation of substrates to lactic acid. The catalysts with acidity, basicity, or acidity-basicity can catalyze the step reactions as mentioned above to give lactic acid.

Table 2.1 shows examples of base catalysts for the production of lactic acid or alkyl lactate from several starting reagents and reaction conditions. There are similar reaction steps to obtain lactic acid and alkyl lactate from transformation of monosaccharides or glycerol. MgO is a solid base catalyst for the conversion of glucose in methanol to obtain methyl lactate (Liu et al., 2011). Compared to $ZrO_2$ and CaO, MgO gives the highest catalytic activity producing methyl lactate yield of 29.45 mol% due to the highest concentration of weakly basic sites. Hydrotalcite, a magnesium-aluminum hydroxycarbonate, is another solid base catalyst which is active for the conversion of glucose to lactic acid in a flow reactor (Onda et al., 2008). The highest yield was 20.3 mol% and the catalytic activity increases linearly with the number of the Brønsted-base sites.

**Table 2.1** Heterogeneous base catalysts for lactic acid or alkyl lactate production.

| Catalyst | Starting reagent | Temperature (°C) | Time (h) | Pressure/ Atmosphere | Catalyst loading (g) | Yield (mol%) | Ref. |
|---|---|---|---|---|---|---|---|
| CaO | glucose | 200 | 20 | - | 0.2 | 0[a] | (Liu et al., 2011) |
| $ZrO_2$ | glucose | 200 | 20 | - | 0.2 | 15.14[a] | (Liu et al., 2011) |
| MgO | glucose | 200 | 20 | - | 0.2 | 29.45[a] | (Liu et al., 2011) |
| Hydrotalcite | glucose | 450 | 6 | 30 mL/min $N_2$ flowing | 0.6 | 20.3 | (Onda et al., 2008) |
| CaO | glycerol | 300 | 1.5 | - | 1.25 M | 7.5 | (Chen et al., 2014) |
| Ca(OH)$_2$ | glycerol | 300 | 1.5 | - | 1.25 M | 7.5 | (Chen et al., 2014) |
| Hydrotalcite | glycerol | 300 | 1.5 | - | 1.25 M | 7.5 | (Chen et al., 2014) |
| $KNO_3/Al_2O_3$ | glycerol | 300 | 1.5 | - | 1.25 M | 7.5 | (Chen et al., 2014) |

a: yield of methyl lactate, -: no data

CaO is a catalyst to transform glycerol to lactic acid compared to alumina loaded with $KNO_3$, $Ca(OH)_2$, and hydrotalcite (Chen et al., 2014). It gives 7.5 mol% lactic acid related to strong basicity. Those solid catalysts have oxygen atoms which act as basic site to activate hydroxyl and carbonyl group in the reaction steps. However, there are side reactions such as oligomerization or C-C cleavage which is not selective to lactic acid.

Table 2.2 shows examples of acid catalysts, heterogeneous catalysts with Brønsted or Lewis acidity on transformation of cellulose to valuable chemicals (Chambon et al., 2011). Brønsted acid catalysts including cesium salts of 12-tungstophosphoric acid ($Cs_2HPW_{12}O_{40}$) and HY zeolite, and Lewis acid catalysts including AlW and ZrW, can transform cellulose to glucose and consequently to lactic acid. The $Cs_2HPW_{12}O_{40}$ and HY zeolite give low lactic acid yield of 3 mol% and its strong Brønsted acid is suggested to be driving force for deep degradation of glucose to levulinic acid and formic acid. The AlW and ZrW are slightly more selective to lactic acid. Additional Lewis acid catalysts are metal modified zeolites. Sn-Beta is another solid acid catalyst for the production of lactic acid from several sugar-based biomass feedstocks including glucose, fructose, sucrose, mannose, and xylose (Sun et al., 2019). Meanwhile, bifunctional solid Pt/Sn-MFI catalyst is reported for lactic acid production from glycerol (Cho et al., 2014). Those Lewis acid catalysts have unsaturated coordination sites which help to undergo several reaction steps.

**Table 2.2** Heterogeneous acid catalysts for lactic acid production.

| Catalyst | Starting reagent | Temperature (°C) | Time (h) | Pressure/ Atmosphere | Catalyst loading (g) | Yield (mol%) | Ref. |
|---|---|---|---|---|---|---|---|
| $Cs_2HPW_{12}O_{40}$ | cellulose | 190 | 24 | 5 MPa He | 0.68 | 3 | Chambon et al., 2011 |
| HY | cellulose | 190 | 24 | 5 MPa He | 0.68 | 3 | Chambon et al., 2011 |
| AlW | cellulose | 190 | 24 | 5 MPa He | 0.68 | 28 | Chambon et al., 2011 |
| ZrW | cellulose | 190 | 24 | 5 MPa He | 0.68 | 19 | Chambon et al., 2011 |
| Sn-Beta | glucose | 200 | 0.5 | 4 MPa He | 0.2 | 57.9 | (Sun et al., 2019) |
| Sn-Beta | sucrose | 200 | 0.5 | 4 MPa He | 0.2 | 54.7 | (Sun et al., 2019) |
| Sn-Beta | fructose | 200 | 0.5 | 4 MPa He | 0.2 | 58.4 | (Sun et al., 2019) |
| Sn-Beta | mannose | 200 | 0.5 | 4 MPa He | 0.2 | 54.1 | (Sun et al., 2019) |
| Sn-Beta | xylose | 200 | 0.5 | 4 MPa He | 0.2 | 67.1 | (Sun et al., 2019) |
| Pt/Sn-MFI | glycerol | 100 | 24 | 0.62 MPa $O_2$ | glycerol/ Pt molar ratio = 350, glycerol/ Sn molar ratio = 226 | 80.5[b] | (Cho et al., 2014) |

b: %selectivity

Both base and acid catalysts can transform sugar or glycerol to lactic acid or alkyl lactate but the yields are low. The higher yields are achieved from metal modified zeolites. However, those modified catalysts may be limited in industrial implementation due to the high cost and long synthesis time impeding scaling up production.

There are also studies of lactic acid production by using acid-base catalysts. Table 2.3 shows examples of acid-base catalysts which are amphoteric metal oxides including

ZnO, $TiO_2$, $SnO_2$, $ZrO_2$, $Y_2O_3$ and $Al_2O_3$ in the lactic acid producing from xylose (Paulino et al., 2018). The Lewis acid-base pair could promote the reaction through the coordination of carbonyl group on Lewis acid site and the coordination of hydroxyl group on Lewis basic site.

**Table 2.3** Heterogeneous acid-base catalysts for lactic acid production.

| Catalyst | Starting reagent | Temperature (°C) | Time (h) | Pressure/ Atmosphere | Catalyst loading (g) | Yield (mol %) | Ref. |
|---|---|---|---|---|---|---|---|
| ZnO | xylose | 160,180 | 0.5 | 30 bar $N_2$ | xylose:catalyst mass ratio = 4 | 26,40 [b] | (Paulino et al., 2018) |
| $TiO_2$ | xylose | 160,180 | 0.5 | 30 bar $N_2$ | xylose:catalyst mass ratio = 4 | 20,20 [b] | (Paulino et al., 2018) |
| $SnO_2$ | xylose | 160,180 | 0.5 | 30 bar $N_2$ | xylose:catalyst mass ratio = 4 | 0,17 [b] | (Paulino et al., 2018) |
| $ZrO_2$ | xylose | 160,180 | 0.5 | 30 bar $N_2$ | xylose:catalyst mass ratio = 4 | 16,9 [b] | (Paulino et al., 2018) |
| $Y_2O_3$ | xylose | 160,180 | 0.5 | 30 bar $N_2$ | xylose:catalyst mass ratio = 4 | 44,50 [b] | (Paulino et al., 2018) |
| $Al_2O_3$ | xylose | 160,180 | 0.5 | 30 bar $N_2$ | xylose:catalyst mass ratio = 4 | 18,18 [b] | (Paulino et al., 2018) |
| 5-20% $ZrO_2$-$Al_2O_3$ | cellulose | 200 | 6 | 0.1 MPa $N_2$ | 1.0 | 21-25 | (Wattanapaphawong et al., 2017) |
| $CuO/Al_2O_3$ | glycerol | 240 | 6 | 14 bar $N_2$ | Cu: 3.5 mmol | 78.6 [b] | (Roy et al., 2011) |
| $\gamma$-$Al_2O_3$ | dihydroxy acetone | 140 | 3 | - | 0.5 | 35 | (Takagaki et al., 2014) |

b: %selectivity, -: no data

Additionally, supported metal oxide catalysts have been developed for different Lewis acid and base site. Wattanapaphawong et al. (2017) have reported that $ZrO_2$-$Al_2O_3$ catalysts have more Lewis acid and less base site than pure $ZrO_2$. The catalytic

activity is compared on conversion of microcrystalline cellulose to lactic acid. The yield from $ZrO_2$-$Al_2O_3$ is higher than that from $ZrO_2$ suggesting that the Lewis acid is more important than base site for retro-aldol condensation which is the key step in this reaction. The supported metal oxide could catalyze not only carbohydrate resource, but also glycerol to lactic acid. Moreover, $CuO/Al_2O_3$ is a good catalyst for glycerol dehydrogenation to glyceraldehyde which is further converted to lactic acid (Roy et al., 2011).

The supported metal oxide are interesting catalysts for lactic acid production from glucose, xylose or glycerol. The presence of acid-base pair on metal oxide surface can inclusively catalyze several reaction steps to transform those substrates into lactic acid. Among many acid-base metal oxides, gamma-alumina ($\gamma$-$Al_2O_3$) is a promising catalyst and support.

$\gamma$-$Al_2O_3$ is one of transition aluminas which is traditionally considered as a cubic defect spinel structure. The oxygen anions arrange to cubic close-packed stacking whereas aluminum cations occupy in the octahedral and tetrahedral sites. It is a low-cost solid catalyst with high surface area and thermal stability. It has become one of the most important catalysts and supports in many reactions (Euzen et al., 2002).

There are a few reports on the use of $\gamma$-$Al_2O_3$ on lactic acid production. Takagaki et al. (2014) have investigated the catalytic activity of $\gamma$-$Al_2O_3$ on dihydoxyacetone to lactic acid in an aqueous solution. The conversion of 91% and lactic acid selectivity of 35% are higher than those from other metal oxides such as $SnO_2$, $TiO_2$ and $WO_2$. Yamaguchi et al. (2018) have reported that $\gamma$-$Al_2O_3$ could convert dihydoxyacetone and glucose to methyl lactate in methanol solution. They have suggested that the high density of both acid and base functionalities is essential to promote many reaction steps

such as isomerization, retro-aldol condensation, and dehydration reactions.

Moreover, $\gamma$-$Al_2O_3$ has been used as a catalyst support, for examples, Sn/$\gamma$-$Al_2O_3$ for glucose isomerization to fructose (Yatoo and Saravanamurugan, 2019) and glucose conversion to lactic acid (Marianou et al., 2018), Au/$\gamma$-$Al_2O_3$ for glycerol oxidation to lactic acid (Ntho et al., 2013), and Pt/$\gamma$-$Al_2O_3$ for glycerol oxidation to glyceraldehyde (Roz et al., 2019).

From the literature review above, it is proposed in this thesis to use $\gamma$-$Al_2O_3$ as a catalyst and support in the transformation of xylose, glucose, and glycerol to lactic acid.

Moreover, the catalyst acidity can be enhanced by dispersing metal oxide on $\gamma$-$Al_2O_3$ to enhance the lactic acid formation. Wattanapaphawong et al. (2017) have suggested that Lewis acid is more important than base site for the retro-aldol condensation which is the key step to obtain lactic acid from xylose and glucose. Wang et al. (2019) have studied metal oxides ($SnO_2$, $Al_2O_3$, $PbO$, $CdO$ or $Cr_2O_3$) modified $Nb_2O_5$ for conversion of dihydroxylacetone to lactic acid. The yield of lactic acid is directly proportional to total acidity. Hence, it is proposed in this thesis to modify $\gamma$-$Al_2O_3$ with another metal oxides to provide high activity on the transformation of xylose, glucose, and glycerol to lactic acid.

The motivation to modify $\gamma$-$Al_2O_3$ with various metal species is based on their known activity as homogeneous catalysts. Rasrendra et al. (2011) have applied compound of Co, Ni, Cu, Zn, Na, Mg, Fe, La, Zn, Sn, Cr and Al to produce lactic acid from dihydroxyacetone. They have screened 26 metal salts and found that the salts of Cu, Co, Ni, Sn, Cr and Al provided more than 70% conversion of dihydroxyacetone after 90 min. High yields of lactic acid (80-92%) are obtained from the salts of Cr and Al. Moderate yields (20-30%) are obtained from the salts of Ni and Sn and very low

yields ($< 5\%$) are obtained from the salts of other metal. They have suggested that the metal ions act as Lewis acid catalysts by coordination and activation of the carbonyl group.

Moreover, compounds of Cu, Co, Ni, Sn, Cr and Al are used to produce lactic acid or alkyl lactate from various starting material including cellulose, derivative carbohydrates and raw biomasses. Hayashi and Sasaki (2005) have demonstrated the conversion of C3 monosaccharides to alkyl lactates using Sn halides in alcoholic solvents. $SnCl_2$ converted dihydroxyacetone, glyceraldehyde and pyruvic aldehyde in methanol to methyl lactate with high yields (89%, 85% and 88%, respectively). They have reported that $CrCl_3 \cdot 6H_2O$ and $AlCl_3 \cdot 6H_2O$ give moderate yields, 50% and 62%, respectively. They have proposed that the metal species simply act as a Lewis acid for activation of carbonyl compound to give a hemi-acetal derivative as an intermediate which could react with alcohol. The reaction is followed by 1,2-hydride shift from the terminal carbon to the central one to alkyl lactate. This reaction can be extended for the direct conversion of larger sugars such as monosaccharide (i.e., glucose and fructose) and oligosaccharide (i.e., cellulose) to alkyl lactates. Bicker et al. (2005) have reported that Co(II), Ni(II) and Cu(II) are applied for conversion of both C3 and C6 monosaccharides to lactic acid under sub- and supercritical water. The addition of a small amount of metal ion to the reaction can increase the yield of lactic acid. Furthermore, Kong et al. (2008) have reported the use of Co, Ni and Cr ions to produce lactic acid from raw biomass such as maize straw, sawdust and rice husk. The lactic acid yield of 27-88% is obtained within 2 min.

Even though the homogeneous catalysts from Cu, Co, Cr, Ni and Sn have shown a good performance providing a fast reaction rate, they are corrosive to reactor, difficult

to reuse and could contaminate the environment. Those problems could be overcome by dispersing those metal species on support to produce heterogeneous catalysts. Therefore, the motivation of this work is to bring those metal species dispersing on $\gamma$-$Al_2O_3$ and Sn, Cu, Co, Cr and Ni are selected to increase acidity on the catalysts in this thesis.

## 2.5 References

Alves de Oliveira, R., Komesu, A., Vaz Rossell, C. E., and Maciel Filho, R. (2018). Challenges and opportunities in lactic acid bioprocess design from economic to production aspects. **Biochemical Engineering Journal**. 133: 219-239.

Bicker, M., Endres, S., Ott, L., and Vogel, H. (2005). Catalytical conversion of carbohydrates in subcritical water: A new chemical process for lactic acid production. **Journal of Molecular Catalysis A: Chemical**. 239(1-2): 151-157.

Chambon, F., Rataboul, F., Pinel, C., Cabiac, A., Guillon, E., and Essayem, N. (2011). Cellulose hydrothermal conversion promoted by heterogeneous Brønsted and Lewis acids : Remarkable efficiency of solid Lewis acids to produce lactic acid. **Applied Catalysis B: Environmental**. 105(1-2): 171-181.

Chen, L., Ren, S., and Ye, X. P. (2014). Lactic acid production from glycerol using CaO as solid base catalyst. **Fuel Processing Technology**. 120: 40-47.

Cho, H. J., Chang, C. C., and Fan, W. (2014). Base free, one-pot synthesis of lactic acid from glycerol using a bifunctional Pt/Sn-MFI catalyst. **Green Chemistry**. 16(7): 3428-3433.

Dai, C., Sun, L., Liao, H., Khezri, B., Webster, R. D., Fisher, A. C., and Xu, Z. J. (2017). Electrochemical production of lactic acid from glycerol oxidation catalyzed by

AuPt nanoparticles. **Journal of Catalysis**. 356: 14-21.

Datta, R. and Henry, M. (2006). Lactic acid: recent advances in products, processes and technologies-a review. **Journal of Chemical Technology and Biotechnology**. 81(7): 1119-1129.

Deng, W., Wang, P., Wang, B., Wang, Y., Yan, L., Li, Y., Zhang, Q., Cao, Z., and Wang, Y. (2018). Transformation of cellulose and related carbohydrates into lactic acid with bifunctional Al(III)-Sn(II) catalysts. **Green Chemistry**. 20(3): 735-744.

Deng, W., Zhang, Q., and Wang, Y. (2015). Catalytic transformations of cellulose and its derived carbohydrates into 5-hydroxymethylfurfural, levulinic acid, and lactic acid. **Science China Chemistry**. 58(1): 29-46.

El Roz, A., Fongarland, P., Dumeignil, F., and Capron, M. (2019). Glycerol to glyceraldehyde oxidation reaction over Pt-based catalysts under base-free conditions. **Frontiers in Chemistry**. 7: 1-9.

Euzen, P., Raybaud, P., Krokidis, X., Toulhoat, H., Le Loarer, J.-L., Jolivet, J.-P., and Froidefond, C. (2002). 4.7.2. Alumina. Handbook of Porous Solids, 3, Schüth F., Sing K.S.W., Weitkamp J. (eds),**Wiley-VCH Verlag GmbH, Weinheim**.

Feliczak-Guzik, A., Sprynskyy, M., Nowak, I., and Buszewski, B. (2018). Catalytic isomerization of dihydroxyacetone to lactic acid and alkyl lactates over hierarchical zeolites containing tin. **Catalysts**. 8: 31-43.

Ferrini, P., Dijkmans, J., De Clercq, R., Van de Vyver, S., Dusselier, M., Jacobs, P. A., and Sels, B. F. (2017). Lewis acid catalysis on single site Sn centers incorporated into silica hosts. **Coordination Chemistry Reviews**. 343: 220-255.

Gupta, B., Revagade, N., and Hilborn, J. (2007). Poly(lactic acid) fiber: An overview. **Progress in Polymer Science**. 32(4): 455-482.

Hayashi, Y. and Sasaki, Y. (2005). Tin-catalyzed conversion of trioses to alkyl lactates in alcohol solution. **Chemical Communications**. 21: 2716-2718.

Komesu, A., Allan Rocha de Oliveira, J., Helena da Silva Martins, L., Regina Wolf Maciel, M., and Maciel Filho, R. (2017). Lactic acid manufacture. **BioResources**. 12(2): 4364-4383.

Kong, L., Li, G., Wang, H., He, W., and Ling, F. (2008). Hydrothermal catalytic conversion of biomass for lactic acid production. **Journal of Chemical Technology and Biotechnology**. 83(3): 383-388.

Liu, Z., Li, W., Pan, C., Chen, P., Lou, H., and Zheng, X. (2011). Conversion of biomass-derived carbohydrates to methyl lactate using solid base catalysts. **Catalysis Communications**. 15(1): 82-87.

Marianou, A. A., Michailof, C. M., Pineda, A., Iliopoulou, E. F., Triantafyllidis, K. S., and Lappas, A. A. (2018). Effect of Lewis and BrØnsted acidity on glucose conversion to 5-HMF and lactic acid in aqueous and organic media. **Applied Catalysis A: General**. 555(2010): 75-87.

Ntho, T., Aluha, J., Gqogqa, P., Raphulu, M., and Pattrick, G. (2013). Au/γ-Al$_2$O$_3$ catalysts for glycerol oxidation: The effect of support acidity and gold particle size. **Reaction Kinetics, Mechanisms and Catalysis**. 109: 133-148.

Onda, A., Ochi, T., Kajiyoshi, K., and Yanagisawa, K. (2008). Lactic acid production from glucose over activated hydrotalcites as solid base catalysts in water. **Catalysis Communications**. 9(6): 1050-1053.

Paulino, P. N., Reis, O. C., Licea, Y. E., Albuquerque, E. M., and Fraga, M. A. (2018). Valorisation of xylose to lactic acid on morphology-controlled ZnO catalysts. **Catalysis Science and Technology**. 8(19): 4945-4956.

Rasrendra, C. B., Fachri, B. A., Makertihartha, I. G. B. N., Adisasmito, S., and Heeres, H. J. (2011). Catalytic conversion of dihydroxyacetone to lactic acid using metal salts in water. **ChemSusChem**. 4(6): 768-777.

Roy, D., Subramaniam, B., and Chaudhari, R. V. (2011). Cu-based catalysts show low temperature activity for glycerol conversion to lactic acid. **ACS Catalysis**. 1(5): 548-551.

Sun, Y., Shi, L., Wang, H., Miao, G., Kong, L., Li, S., and Sun, Y. (2019). Efficient production of lactic acid from sugars over Sn-Beta zeolite in water: Catalytic performance and mechanistic insights. **Sustainable Energy and Fuels**. 3(5): 1163-1171.

Taarning, E., Saravanamurugan, S., Holm, M. S., Xiong, J., West, R. M., and Christensen, C. H. (2009). Zeolite-catalyzed isomerization of triose sugars. **ChemSusChem**. 2(7): 625-627.

Takagaki, A., Jung, J. C., and Hayashi, S. (2014). Solid Lewis acidity of boehmite $\gamma$-AlO(OH) and its catalytic activity for transformation of sugars in water. **RSC Advances**. 4(82): 43785-43791.

Wang, X., Song, Y., Huang, L., Wang, H., Huang, C., and Li, C. (2019). Tin modified $Nb_2O_5$ as an efficient solid acid catalyst for the catalytic conversion of triose sugars to lactic acid. **Catalysis Science and Technology**. 9(7): 1669-1679.

Wattanapaphawong, P., Sato, O., Sato, K., Mimura, N., Reubroycharoen, P., and Yamaguchi, A. (2017). Conversion of cellulose to lactic acid by using $ZrO_2$-$Al_2O_3$ **Catalysts. Catalysts**. 7(7): 221-231.

Xia, M., Dong, W., Gu, M., Chang, C., Shen, Z., and Zhang, Y. (2018). zeolite for lactic acid synthesis from biomass- derived carbohydrates. **RSC Advances**. 8: 8965-

8975.

Yamaguchi, S., Yabushita, M., Kim, M., Hirayama, J., Motokura, K., Fukuoka, A., and Nakajima, K. (2018). Catalytic conversion of biomass-derived carbohydrates to methyl lactate by acid-base bifunctional γ-Al$_2$O$_3$. **ACS Sustainable Chemistry and Engineering**. 6(7): 8113-8117.

Yang, L., Su, J., Carl, S., Lynam, J. G., Yang, X., and Lin, H. (2015). Catalytic conversion of hemicellulosic biomass to lactic acid in pH neutral aqueous phase media. **Applied Catalysis B: Environmental**. 162: 149-157.

Yang, L., Yang, X., Tian, E., Vattipalli, V., Fan, W., and Lin, H. (2016). Mechanistic insights into the production of methyl lactate by catalytic conversion of carbohydrates on mesoporous Zr-SBA-15. **Journal of Catalysis**. 333: 207-216.

Yatoo, M. A., and Saravanamurugan, S. (2019). Tin grafted on modified alumina-catalyzed isomerisation of glucose to fructose. **Applied Catalysis A: General**. 582: 117094-117111.

# CHAPTER III

# EXPERIMENTAL

## 3.1 Chemicals

Chemicals used in this research are listed in Table 3.1.

**Table 3.1** Chemicals used in this research.

| Chemicals | Formula | Content (%) | Suppliers |
|---|---|---|---|
| boehmite aluminium oxide | $\gamma$-AlO(OH) | - | SASOL |
| cobalt nitrate | $Co(NO_3)_2 \cdot 6H_2O$ | 99% | Ajax Finechem |
| copper nitrate | $Cu(NO_3)_2 \cdot 3H_2O$ | 99% | Ajax Finechem |
| chromium nitrate | $Cr(NO_3)_3 \cdot 9H_2O$ | 98% | HIMEDIA |
| nickel nitrate | $Ni(NO_3)_2 \cdot 6H_2O$ | 99% | Ajax Finechem |
| tin chloride | $SnCl_2 \cdot 2H_2O$ | 98% | Sigma Aldich |
| d-xylose | $HOCH_2(CH(OH))_3CHO$ | 98% | Sigma Aldich |
| dl-lactic acid | $C_2H_4OHCOOH$ | 90% | Sigma Aldrich |
| furfural | $C_4H_3OCHO$ | 99% | Sigma Aldrich |

## 3.2 Preparation of metal oxide supported alumina catalyst

Gamma-alumina ($\gamma$-$Al_2O_3$) was prepared according to Wang et al. (2018) by calcination of boehmite at 450 °C for 3 h under a heating rate of 5 °C/min. All supported metal oxide catalysts were prepared by wet impregnation method with 10 wt% metal loading. For example, $Co/Al_2O_3$ was prepared by stirring $\gamma$-$Al_2O_3$ in a solution of $Co(NO_3)_2 \cdot 6H_2O$ before drying at 60 °C in a vacuum oven overnight.

Then, the dried powder was ground and calcined 550 °C for 4 h with a heating rate of 5 °C/min.

## 3.3 Catalyst characterization

Phases of γ-Al$_2$O$_3$ and supported metal oxide samples were investigated by X-ray diffraction (XRD) on a Bruker D8 ADVANCE with a monochromatic light source Cu K$_\alpha$ radiation (λ = 1.5418 Å) operated at the voltage and current of 40 kV and 40 mA. The samples were analyzed using a scan speed 0.5 s/step and increment 2.0 s/step. Before the measurement, each sample powder was spread evenly in the sample holder and pressed by glass to produce a smooth surface. The average crystallite site of γ-Al$_2$O$_3$ was calculated using Scherrer equation: $\tau = \frac{K\lambda}{\beta \cos\theta}$, where: $\tau$ is the mean size of the ordered (crystalline) domains, which may be smaller or equal to the grain size. K is a Scherrer constant which varies from 0.68-2.08 with the actual shape of the crystallite (0.94 in this work). λ is the X-ray wavelength. β is the line broadening at half the maximum intensity (FWHM), after subtracting the instrumental line broadening, in radians. This quantity is also sometimes denoted as 2θ; θ is the Bragg angle.

Oxidation state and elemental composition of metal species were determined by X-ray photoelectron spectroscopy (XPS) and X-ray absorption spectroscopy (XAS) at the Beamline 5.2 and 5.3 of the Synchrotron Light Research Institute. For XPS, the calibration of binding energy was carried out by applying C-C bond at B.E. = 284.8 eV as a reference. The sample powder was spread on the carbon tape which stacked on a sample holder. Before measurement, it was vacuumed in the equipment. For XAS, X-ray absorption near edge structure (XANES) measurements were performed at the

K-edge of copper, cobalt, chromium and nickel, and at L-edge of Sn.

Surface area, average pore size, and total pore volume of all samples were determined by nitrogen adsorption-desorption analysis. Nitrogen adsorption-desorption isotherms were obtained from a NOVA 2000e surface area and pore size analyzer. Before analysis, about 0.5 g of each sample was degassed at 250 °C under vacuum for 2 h and left until the pressure reached $10^{-2}$ mPa in order to remove physisorbed gases. The analysis was carried out at -196 °C at relative pressure (P/P$_0$) from 0.01 to 0.99. The surface area was calculated by Brunauer-Emmett-Teller (BET) method. The total pore volume was determined from the nitrogen amount adsorbed in correspondence of P/P$_0$ equal to 0.99, and the pore size distribution was calculated by Barrett-Joyner-Halenda (BJH) method.

Morphology of catalysts was studied by scanning electron microscopy (SEM) (Auriga Carl Zeiess). The sample powder was spread on a layer of carbon tape adhered on a metal stub and coated by gold under an argon atmosphere to make them electrically conduct before took the SEM images. Its elemental composition was analyzed by energy dispersive spectroscopy (EDS) technique.

Morphology of catalysts was further studied by transmission electron microscopy (TEM) which was performed on a Tecnai G$^2$ with an accelerating voltage of 200 kV. The samples were suspended in 95% ethanol solution with sonication. The suspension was deposited on a micro grid with a holey carbon copper as a support membrane and dried at 70 °C with a UV lamp.

Acidity of catalysts was determined by temperature-programmed desorption of ammonia (NH$_3$-TPD) using a Belcat-B equipped with a thermal conductivity detector. The sample 0.05 g was taken into the U-type glass cell and pretreated at 250 °C

(10 °C/min) under He flow (50 mL/min) for 30 min in the equipment. After that, the sample was cooled to 50 °C and the $NH_3$ was adsorbed by flowing 50 mL/min of $NH_3$/He for 30 min. The He gas was purged again for 15 min to flush out excess $NH_3$ gas from the cell. Then, $NH_3$-TPD measurements were carried out up to 800 °C with the heating rate of 10 °C/min under He flow (30 mL/min).

Basicity of catalysts was determined by temperature-programmed desorption of carbon dioxide ($CO_2$-TPD) using a Belcat-B equipped with a thermal conductivity detector. The sample (0.05 g) was put into the U-type glass cell and pretreated at 500 °C (10 °C/min) under He flow (50 mL/min) for 1 h in the equipment. After that, the sample was cooled to 50 °C and the $CO_2$ was adsorbed by flowing 50 mL/min of $CO_2$/He for 30 min. The He gas was purged again for 1 h to flush out excess $NH_3$ gas from the cell. Then, $CO_2$-TPD measurements were carried out up to 800 °C with the heating rate of 10 °C/min under He flow (30 mL/min).

## 3.4 Catalytic testing in xylose conversion to lactic acid

All catalysts were tested in a stainless-steel batch reactor with an inner Teflon container (75 mL). In a typical experiment, D-xylose (0.9 g), deionized (DI) water (30 mL), catalyst (0.5 g) were added into the Teflon container. The reactor was filled with nitrogen gas to 5 bar and released repeatedly for three times to remove air. Then it was pressurized to 15 bar with nitrogen gas and heated to 170 °C under magnetic stirring with a speed of 750 rpm. During the reaction time of 6 h, the sample (approximately 1 mL) was taken every hour, filtered through a 0.22 µm Nylon filter membrane, and analyzed by high-performance liquid chromatography (HPLC, Shimadzu, SPD-20A) equipped with a UV-Vis and refractive index detectors. The HPLC column was Aminex

HPX-87H from Bio-Rad. The mobile phase was 5 mM $H_2SO_4$ with 0.6 mL/min flow rate and the column temperature was 45 °C.

**Calculation:**

$$\text{Conversion (\%)} = \frac{\text{Initial moles of reactant - Final moles of reactant}}{\text{Initial moles of reactant}} \times 100$$

$$\text{Lactic acid yield (\%)} = \frac{\text{Moles of carbon atoms in lactic acid}}{\text{Moles of carbon atoms in convert reactant}} \times 100$$

## 3.5 Reference

Wang, Y., Yang, J., Gu, R., Peng, L., Guo, X., Xue, N., Zhu, Y., and Ding, W. (2018). Crystal-facet effect of γ-$Al_2O_3$ on supporting $CrO_x$ for catalytic semihydrogenation of acetylene. **ACS Catalysis**. 8(7): 6419-6425.

# CHAPTER IV

# RESULTS AND DISCUSSION

## 4.1 Sample characterizations

### 4.1.1 Phase analysis by X-ray diffraction (XRD)

XRD patterns of bare $\gamma$-$Al_2O_3$ and alumina-supported metal species are shown in Figure 4.1. The $\gamma$-$Al_2O_3$ shows its characteristic peaks (PDF 00-001-1303, Wang et al., 2018). The crystallite size calculated via Scherrer equation is around 5 nm. The XRD result confirmed that boehmite was transformed to gamma-alumina by calcination at 450 °C. All supported catalysts also showed the phase of $\gamma$-$Al_2O_3$ indicating that the phase of the support did not change after the preparation procedure. Moreover, all catalysts except $Cr/Al_2O_3$ sample showed diffraction peaks of each metal oxides or mixed phase, namely, CuO (PDF 01-077-7716), $Co_3O_4$ (PDF 00-043-1003), NiO (PDF 00-047-1049) mixed with $NiAl_2O_4$ (PDF 01-081-0711), and $SnO_2$ (PDF 01-070-6153). For $Cr/Al_2O_3$, the peaks of any compound were not observed implying that it has amorphous phase and/or good dispersion. According to the literature (Wang et al., 2018), $Cr(NO_3)_2 \cdot 9H_2O$ on $\gamma$-$Al_2O_3$ was transformed to $Cr_xO_y$ with consisted of $Cr^{3+}$ and $Cr^{6+}$ species by calcination at 550 °C for 3 h. With the similar calcination temperature and longer time in $Cr/Al_2O_3$, $Cr_xO_y$ contained $Cr^{3+}$ and $Cr^{6+}$ species was also expected in this work. To ensure the form of chromium species, the $Cr/Al_2O_3$ sample was further analyzed by XPS.
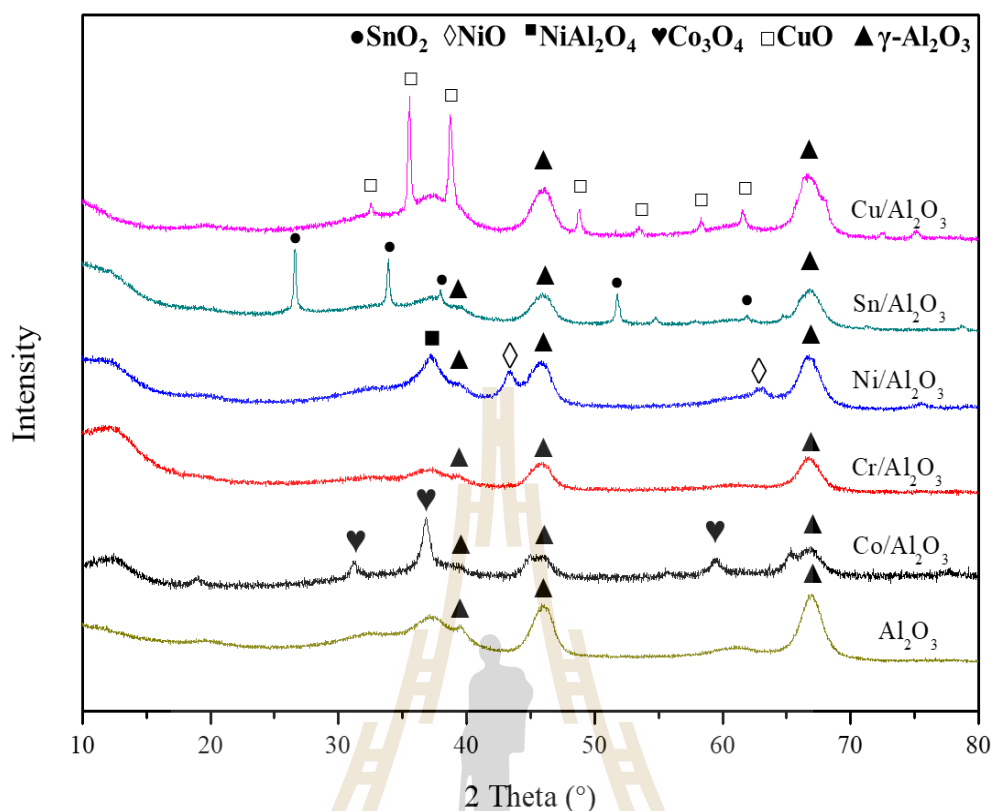
**Figure 4.1** XRD patterns of metal species supported on $Al_2O_3$ prepared via impregnation method with 10 wt% metal loading and calcined in a muffle furnace at 550 °C for 4 h.

### 4.1.2 XPS and XANES

#### XPS spectra of aluminium

Figure 4.2 shows XPS spectra at Al 2p regions of parent $Al_2O_3$ and all supported metal oxide catalysts. The spectrum of $Al_2O_3$ displays characteristic peak at binding energy 74.22 eV. The Al 2p center spectra from all supported metal oxide catalysts located on the range of 74-75 eV which associated with $\gamma$-$Al_2O_3$ (Strohmeier, 1994). The spectrum of $Co/Al_2O_3$, $Cr/Al_2O_3$, $Ni/Al_2O_3$, $Sn/Al_2O_3$ and $Cu/Al_2O_3$ displays peak at 74.29, 74.12, 74.78, 74.80 and 74.41, respectively. The peaks slightly shift to

higher energy compared to that of the parent $Al_2O_3$. The change of spectrum could from the interaction between $Al_2O_3$ and the added metal oxide.
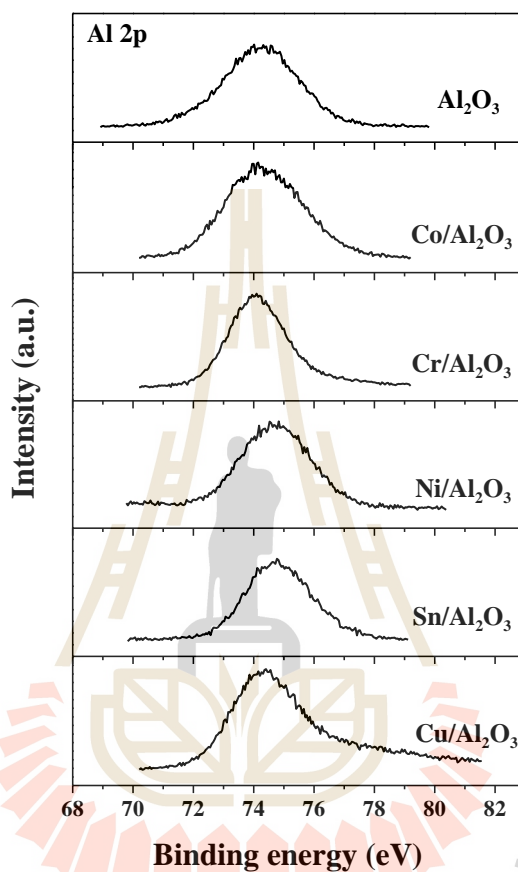


**Figure 4.2** XPS spectrum at Al 2p regions of $Al_2O_3$ and supported catalysts.

### XPS and XANES spectra of metal species

XPS was carried out to identify chemical states and confirm elemental composition of the catalysts. XPS spectra of modified element from all catalysts are shown in Figure 4.3-4.7 and summarized in Table 4.1. The peaks correspond to $Co_3O_4$ (Figure 4.3), NiO and $NiAl_2O_4$ (Figure 4.5), $SnO_2$ (Figure 4.6), CuO and $Cu(OH)_2$ (Akhavan et al., 2011) (Figure 4.7), consistent with the XRD results. The Cr/$Al_2O_3$

sample, the chromium species can not be investigated by XRD, the XPS spectrum (Figure 4.4) indicated the existence of $Cr^{3+}$ and $Cr^{6+}$ species on the catalyst surface. The $Cr^{3+}$ to $Cr^{6+}$ ratio, calculated from fitting peaks of Cr $2p_{3/2}$, was 1.12.
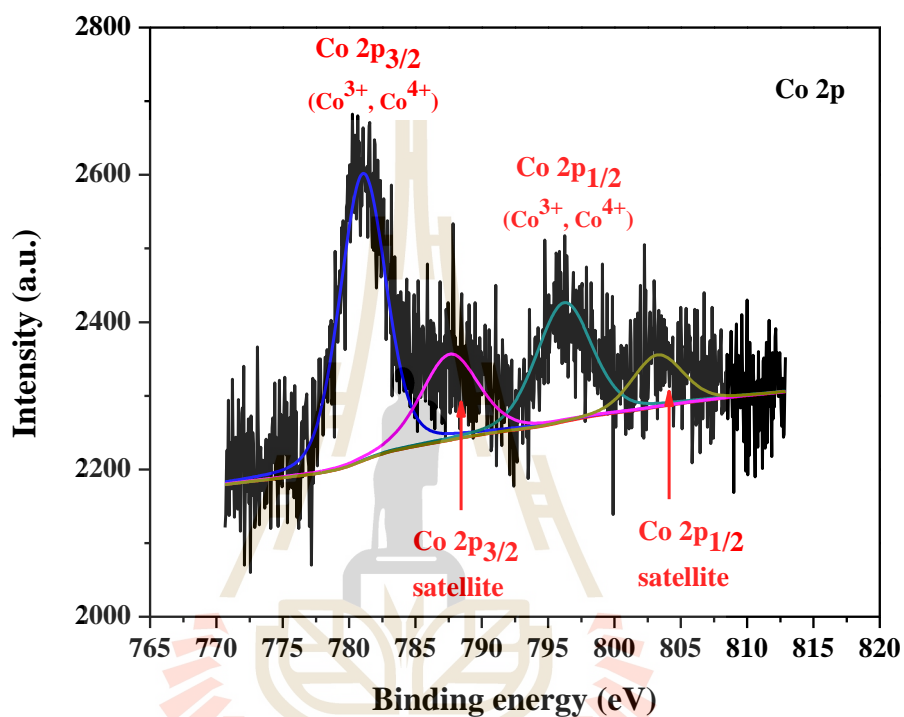


**Figure 4.3** XPS spectrum of $Co/Al_2O_3$.
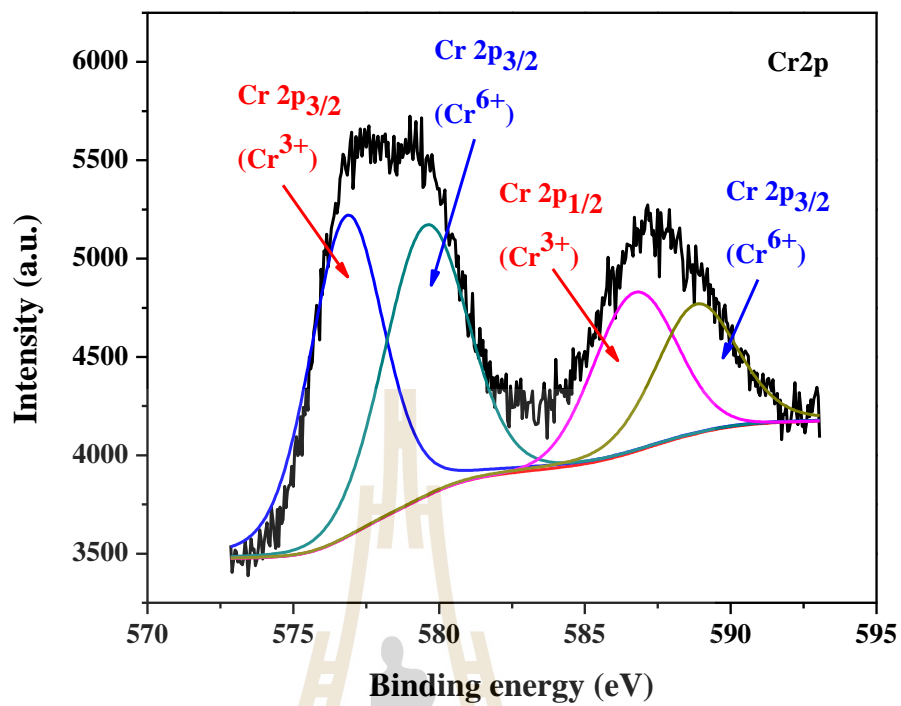
**Figure 4.4** XPS spectrum of Cr/Al$_2$O$_3$.
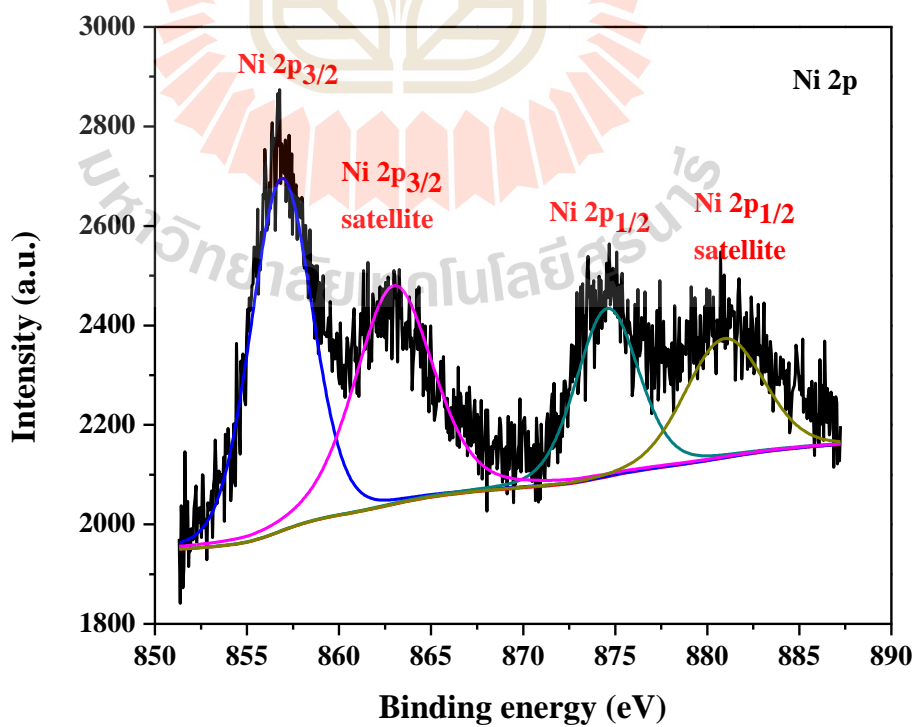


**Figure 4.5** XPS spectrum of Ni/Al$_2$O$_3$.
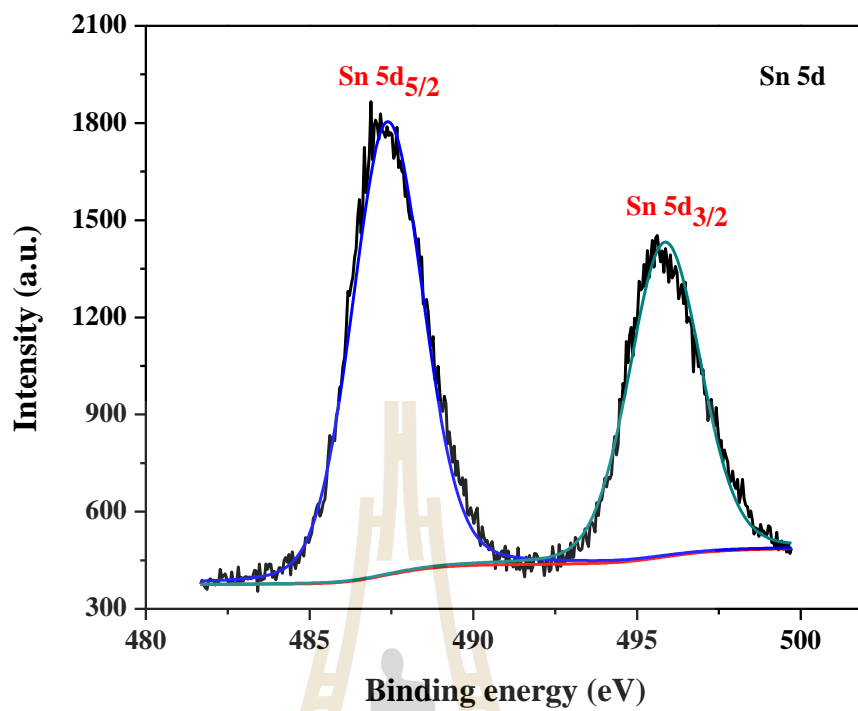
**Figure 4.6** XPS spectrum of Sn/Al$_2$O$_3$.
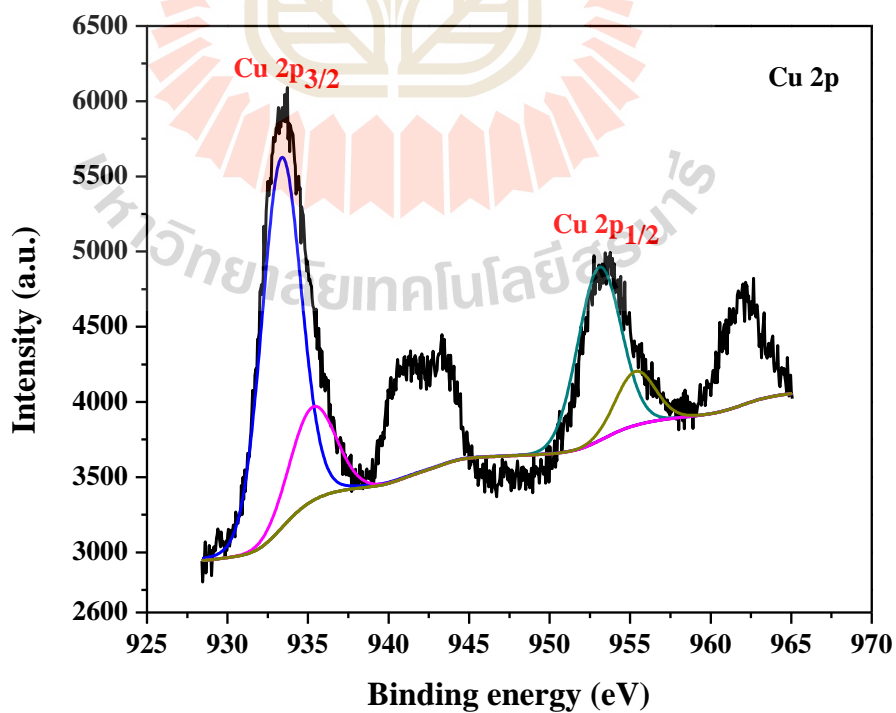


**Figure 4.7** XPS spectrum of Cu/Al$_2$O$_3$.

Table 4.1 shows the binding energies from deconvolution of the XPS spectrums of all supported catalyts. Each metal species has characteristic binding energy associated each core atomic orbitals.

**Table 4.1 Summary of binding energy of each species.**

| Sample | Binding energy (eV) | Orbital | Species | Reference |
|---|---|---|---|---|
| $Co/Al_2O_3$ | 781.03 | Co $2p_{3/2}$ | $Co_3O_4$ | (Yang et al., 2018) |
| | 796.20 | Co $2p_{1/2}$ | | |
| $Cr/Al_2O_3$ | 576.82 | Cr $2p_{3/2}$ | $Cr^{3+}$ | (Wang et al., 2018a) |
| | 586.71 | Cr $2p_{1/2}$ | | |
| | 579.54 | Cr $2p_{3/2}$ | $Cr^{6+}$ | |
| | 588.82 | Cr $2p_{1/2}$ | | |
| $Ni/Al_2O_3$ | 856.87 | Ni $2p_{3/2}$ | NiO, $NiAl_2O_4$ | (Li et al., 2013) |
| | 874.56 | Ni $2p_{1/2}$ | | |
| $Sn/Al_2O_3$ | 487.38 | Sn $3d_{5/2}$ | $SnO_2$ | (Süzer et al., 1996) |
| | 495.85 | Sn $3d_{3/2}$ | | |
| $Cu/Al_2O_3$ | 933.34 | Cu $2p_{3/2}$ | CuO | (Zhou et al., 2010) |
| | 953.08 | Cu $2p_{1/2}$ | | |
| | 935.32 | Cu $2p_{3/2}$ | $Cu(OH)_2$ | (Akhavan et al., 2011) |
| | 955.32 | Cu $2p_{1/2}$ | | |

XANES spectra at the edge of each metal compared with standard materials are shown in Figure 4.8-4.12. The spectra contains the rising absorption edge (white

line) resulted from an absorption energy at core electron equal to or higher than its binding energy. The spectra provides absorption edge energy as characteristic of specific elements in sample. The absorption edge energy and oxidation state of each catalyst and standard materials are summarized in Table 4.2-4.7. The absorption edge energy confirms metal oxidation state which is consistent with the XPS results. The results show that $Co/Al_2O_3$ contains $Co^{2+}$ and $Co^{3+}$, $Cr/Al_2O_3$ contains $Cr^{3+}$ and $Cr^{6+}$, $Ni/Al_2O_3$ contains $Ni^{2+}$, $Sn/Al_2O_3$ contains $Sn^{4+}$ and $Cu/Al_2O_3$ contains $Cu^{2+}$.
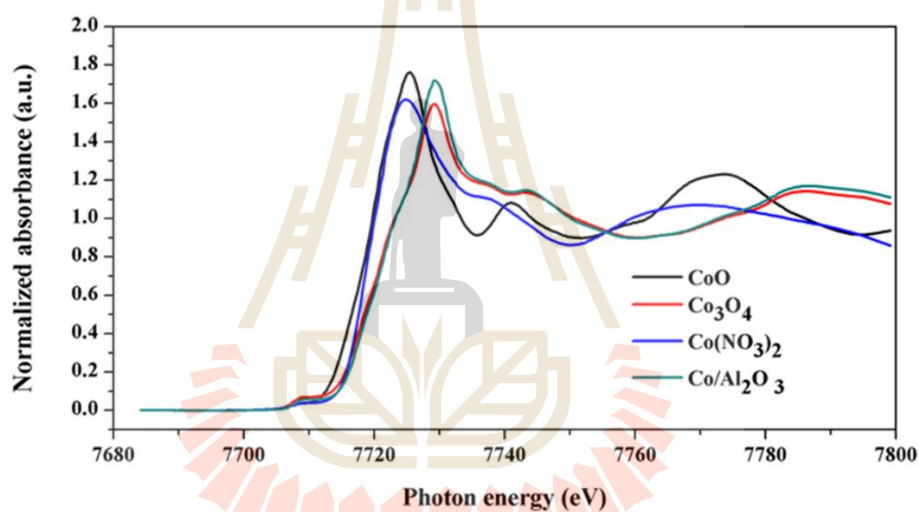


**Figure 4.8 K-edge XANES spectra of cobalt samples.**

**Table 4.2 K-edge energy and oxidation state of cobalt samples.**

| Sample | Absorption edge energy (eV) | Oxidation state |
|---|---|---|
| CoO | 7718.88 | +2 |
| $Co_3O_4$ | 7721.14 | +2,+3 |
| $Co(NO_3)_2$ | 7719.08 | +2 |
| $Co/Al_2O_3$ | 7721.79 | +2,+3 |
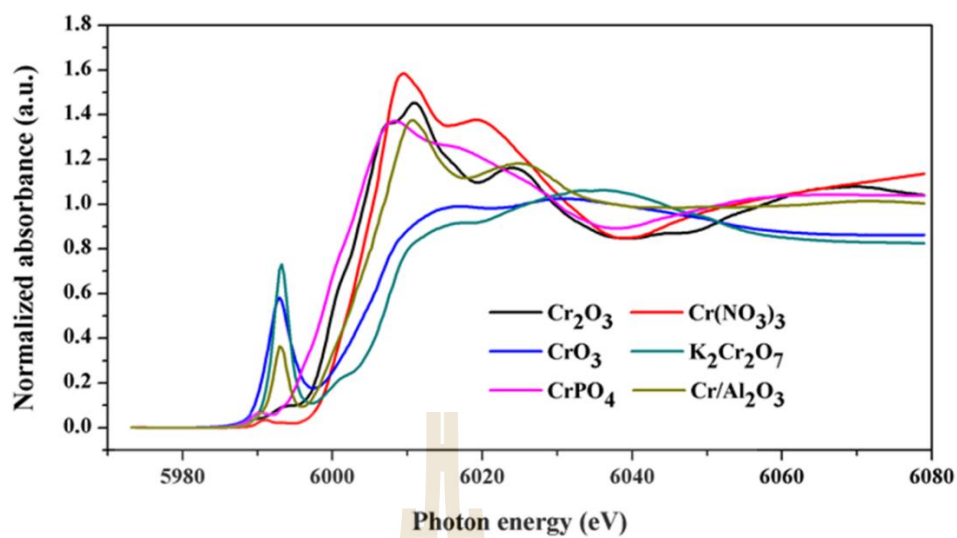
**Figure 4.9 K-edge XANES spectra of chromium samples.**

**Table 4.3 K-edge energy and oxidation state of chromium samples.**

| Sample | Absorption edge energy (eV) | Oxidation state |
|---|---|---|
| $Cr_2O_3$ | 6001.61 | +3 |
| $Cr(NO_3)_3$ | 6003.78 | +3 |
| $CrO_3$ | 5990.96 | +6 |
| $K_2Cr_2O_7$ | 5992.01 | +6 |
| $CrPO_4$ | 5999.56 | +3 |
| $Cr/Al_2O_3$ | 5992.03 | +6 |
| | 6004.50 | +3 |
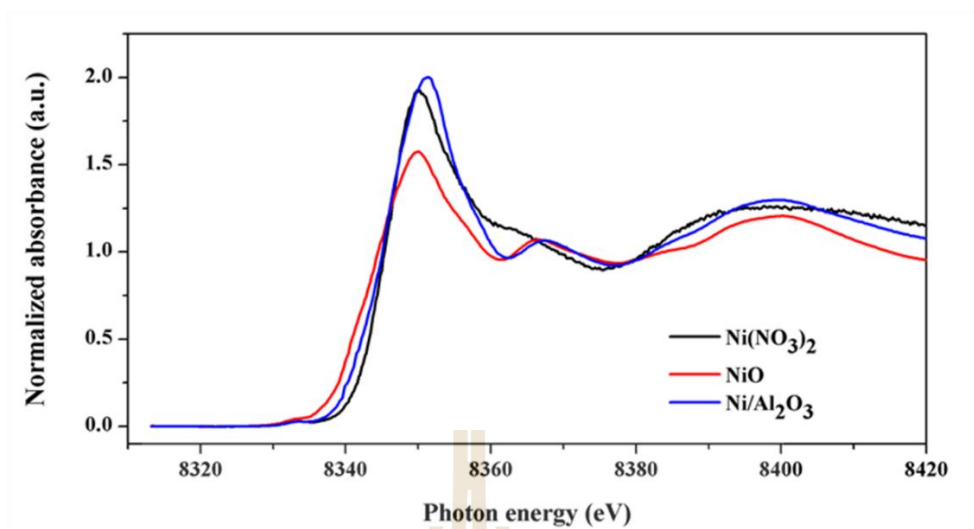
**Figure 4.10 K-edge XANES spectra of nickel samples.**

**Table 4.4 K-edge energy and oxidation state of nickel samples.**

| Sample | Absorption edge energy (eV) | Oxidation state |
|---|---|---|
| NiO | 8343.48 | +2 |
| Ni(NO$_3$)$_2$ | 8345.35 | +2 |
| Ni/Al$_2$O$_3$ | 8345.35 | +2 |
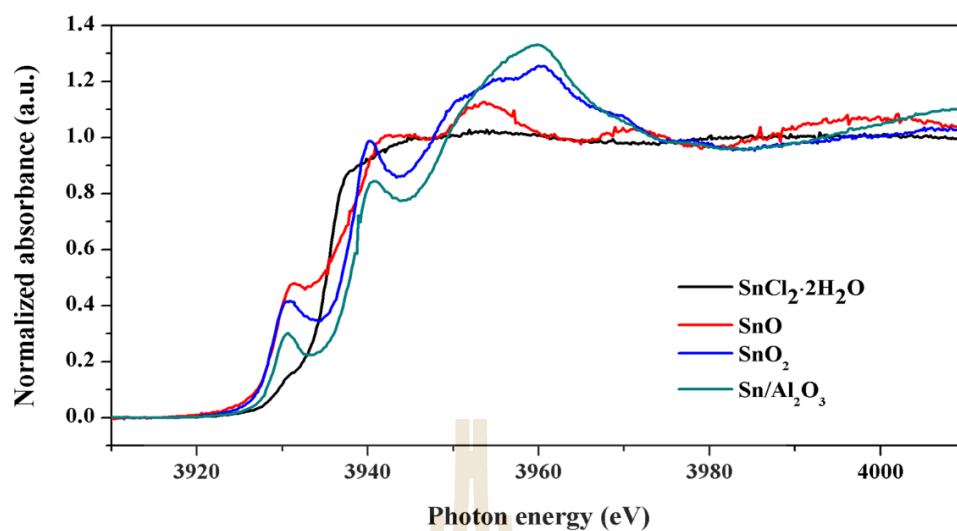
**Figure 4.11 L-edge XANES spectra of tin samples.**

**Table 4.5 L-edge edge energy and oxidation state of tin samples.**

| Sample | Absorption edge energy (eV) | Oxidation state |
|---|---|---|
| $SnO_2$ | 3938.12 | +4 |
| SnO | 3929.04 | +2 |
| $SnCl_2 \cdot 2H O$ | 3935.41 | +2 |
| $Sn/Al_2O_3$ | 3938.39 | +4 |
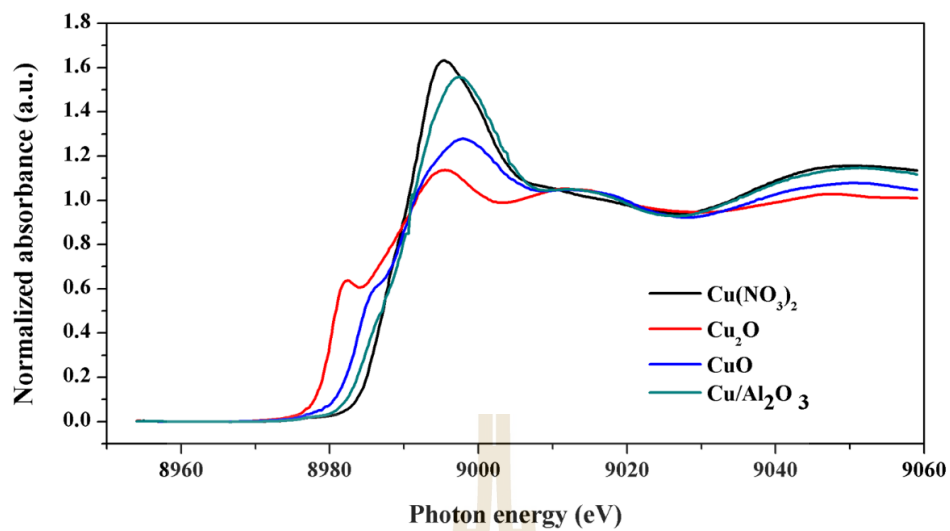
**Figure 4.12 K-edge XANES spectra for copper samples.**

**Table 4.6 Absorption edge energy and oxidation state for copper samples.**

| Sample | Absorption edge energy (eV) | Oxidation state |
|---|---|---|
| $Cu_2O$ | 8980.13 | +2 |
| CuO | 8983.81 | +2 |
| $Cu(NO_3)_2$ | 8989.86 | +2 |
| $Cu/Al_2O_3$ | 8989.86 | +2 |

### 4.1.3 Nitrogen adsorption-desorption analysis

The nitrogen adsorption-desorption isotherms of alumina and all supported samples are displayed in Figure 4.13. According to IUPAC classification (Thommes et al., 2015), the isotherms of all samples are type IV(a) which is characteristic of mesoporous materials. They show type H1 hysteresis loop at a relative pressure range of $P/P_0 = 0.6$-$0.9$ from condensation inside the mesopores. The shape of the hysteresis loop indicate that the mesopores are not uniform. From the pore size distributions in Figure 4.14, all samples have an average pore size of 7.7 nm.

The BET surface areas and pore volumes of all samples as summarized in Table 4.7. The BET surface area of $\gamma$-$Al_2O_3$ compared to the value from the literature (170, 236 or 250 $m^2$/g) is different (Samain et al., 2014; Wang et al., 2018). The difference could be from the different precursors and preparation temperature as reported by Wang et al (2018). After the $Al_2O_3$ is added with metal species, the BET surface areas and pore volumes of the calcined catalysts are similar to each other and slightly smaller than that of the parent $Al_2O_3$. The slight decrease of surface area indicate that the metal oxides disperse well on the surface of $Al_2O_3$. The decrease of the pore volume indicate that the metal oxides distribute inside the pores. The addition of metal oxide did not affect the morphology of the support.
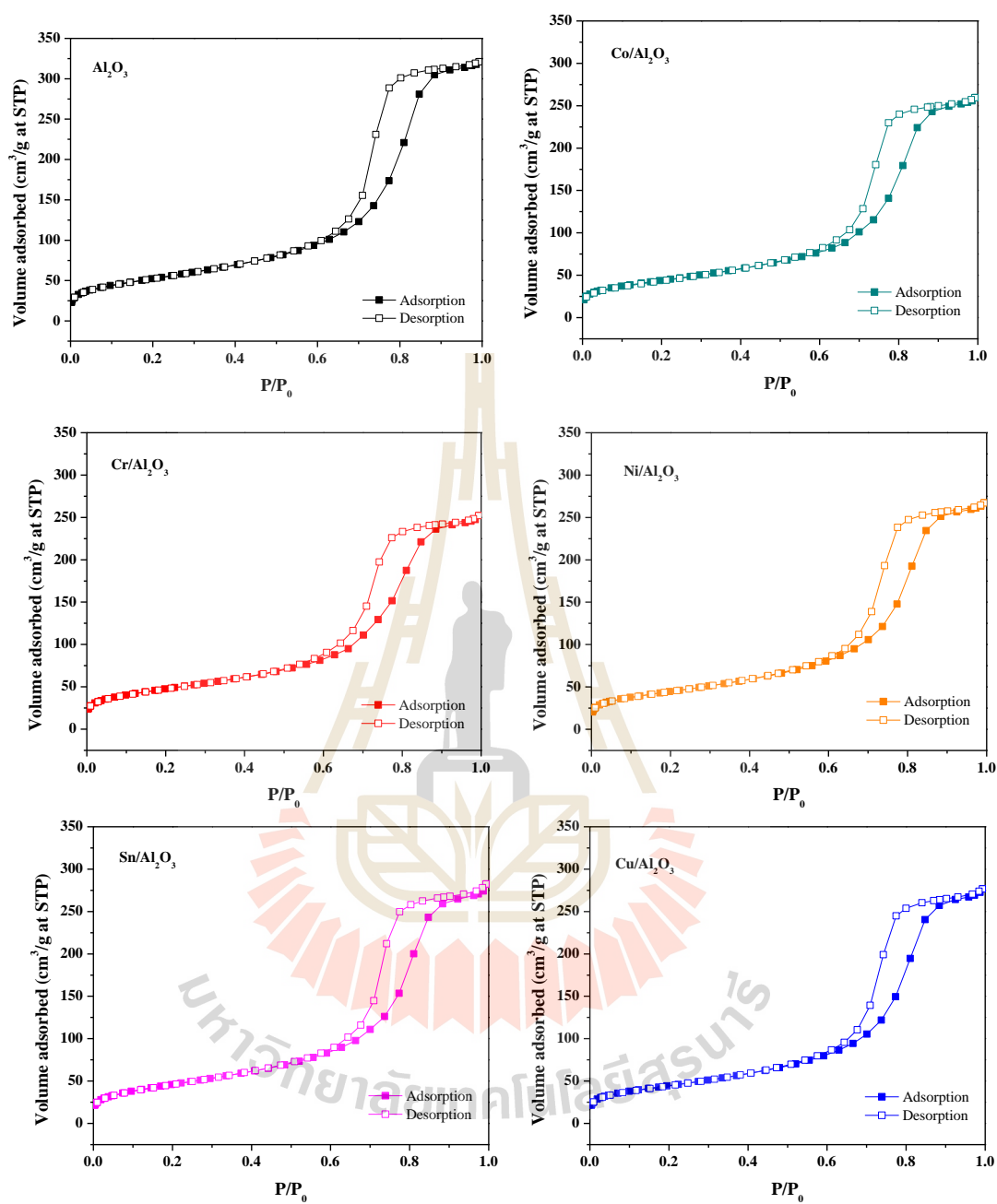
**Figure 4.13** Nitrogen adsorption-desorption isotherms of $Al_2O_3$ and supported

catalysts: $Co/Al_2O_3$, $Cr/Al_2O_3$, $Ni/Al_2O_3$, $Sn/Al_2O_3$, and $Cu/Al_2O_3$.
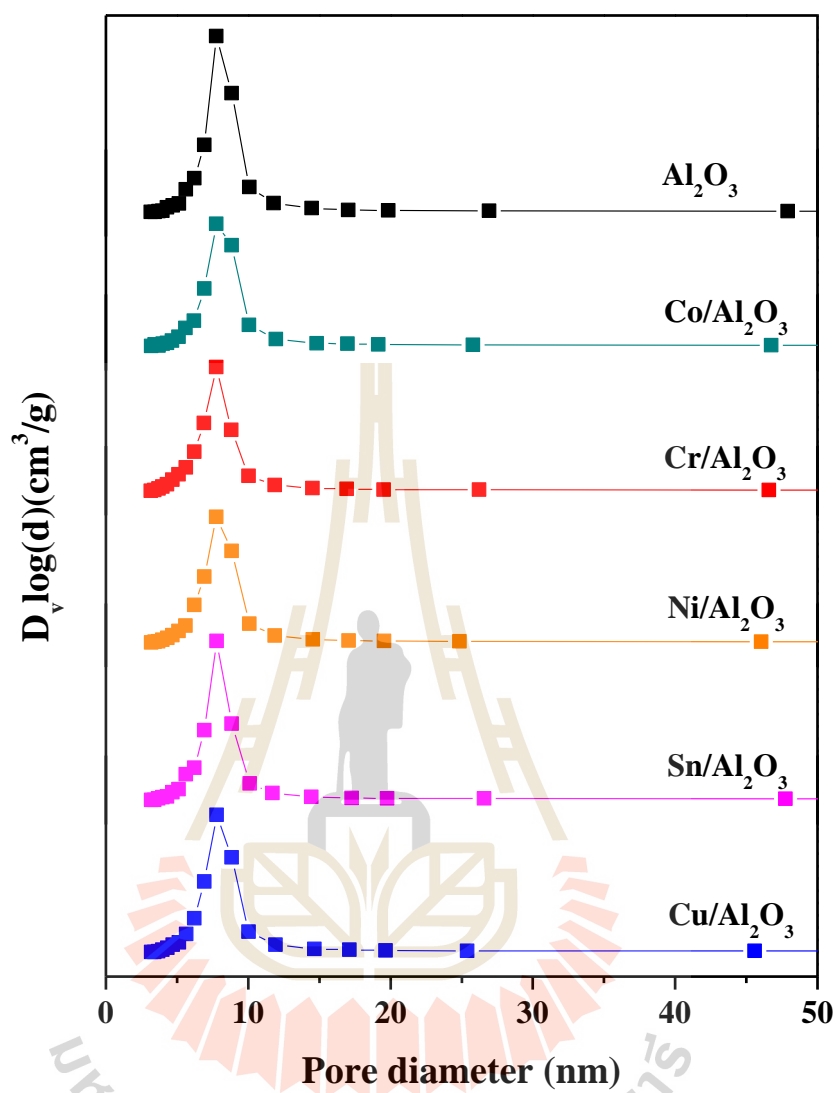
**Figure 4.14** The pore size distribution of $Al_2O_3$ and supported catalysts: Co/ $Al_2O_3$,

Cr/$Al_2O_3$, Ni/$Al_2O_3$, Sn/$Al_2O_3$, and Cu/$Al_2O_3$.

**Table 4.7** BET surface area and pore volume of catalysts.

| Catalyst | BET surface area (m$^2$/g) | Pore volume (cm$^3$/g) |
|---|---|---|
| $Al_2O_3$ | 189 | 0.53 |
| $Co/Al_2O_3$ | 157 | 0.42 |
| $Cr/Al_2O_3$ | 169 | 0.41 |
| $Ni/Al_2O_3$ | 160 | 0.44 |
| $Sn/Al_2O_3$ | 168 | 0.47 |
| $Cu/Al_2O_3$ | 159 | 0.46 |

**4.1.4 Scanning electron microscopy (SEM)**

SEM images of parent $Al_2O_3$ are shown in Figure 4.15. The $Al_2O_3$ has small crystals with irregular shapes and average particle sizes of < 100 μm. Moreover, pores are observed in range of 2-50 nm which can confirm the mesoporous character of γ-$Al_2O_3$. SEM images of metal oxide supported $Al_2O_3$ catalysts are shown in Figure 4.16-4.20. The lighter regions are metal oxide particles whereas the darker regions are $Al_2O_3$ support. The similar porous surface of $Al_2O_3$ is observed from all samples. It can be concluded that the morphology of $Al_2O_3$ is not change after the catalyst preparation. The dispersion of metal oxide on $Al_2O_3$ is not block the pores. These results relate to the BET surface areas which are not significantly different. Furthermore, the elemental

distribution of each samples is determined by SEM/EDX mapping as shown in Figure 4.16-4.20. The mappings confirm that metal oxide species dispersed well on the $Al_2O_3$ surface.
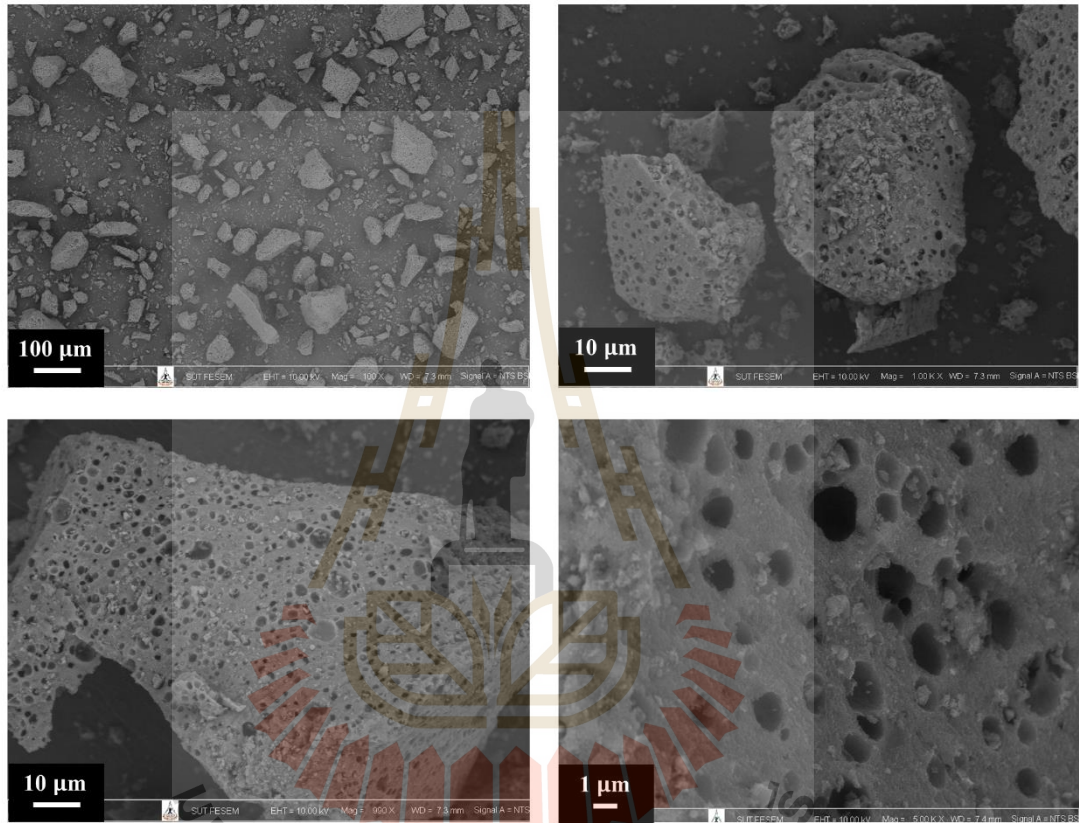


**Figure 4.15** SEM images of $Al_2O_3$ at different magnifications.
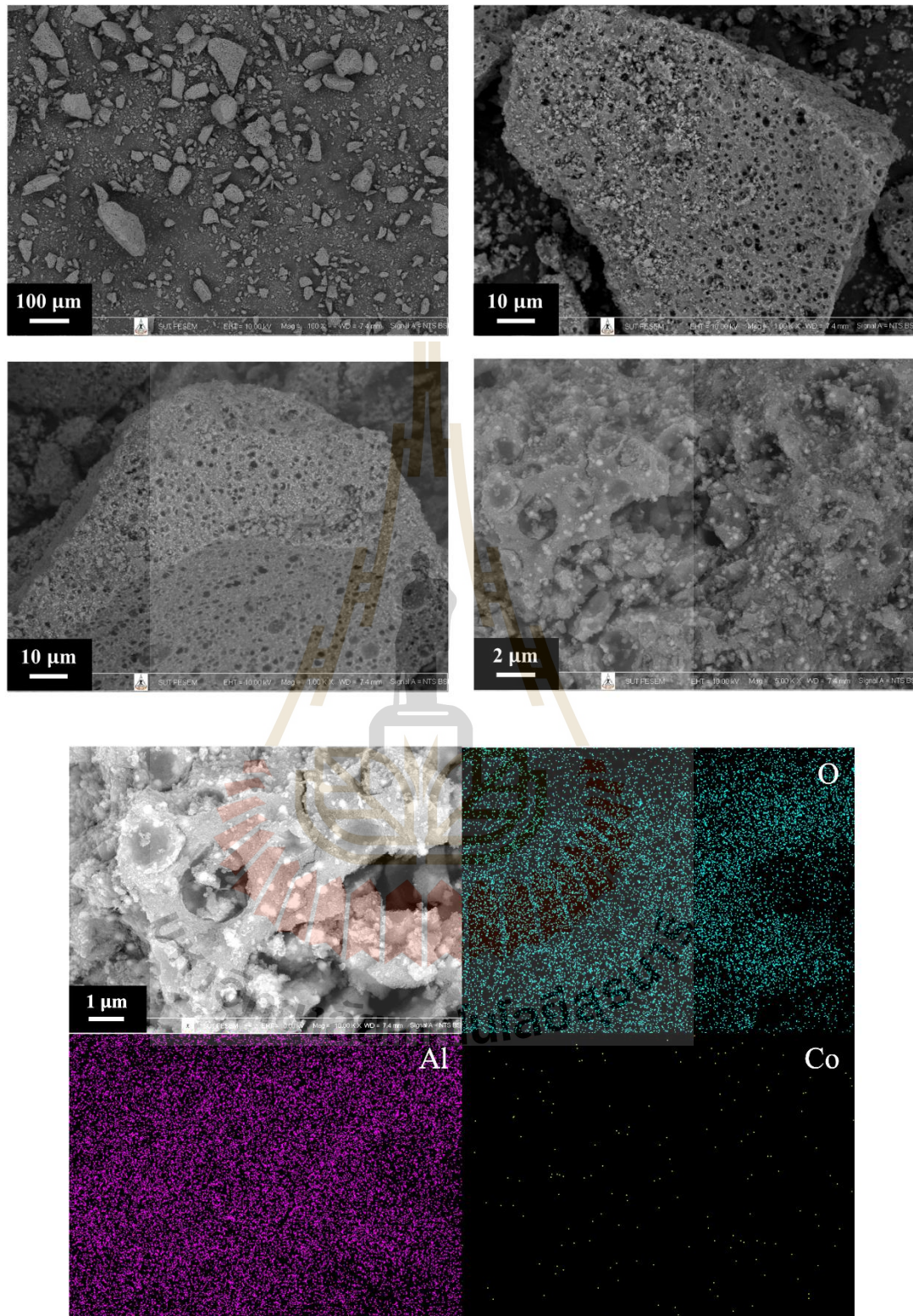
**Figure 4.16** SEM images of Co/Al$_2$O$_3$ at different magnifications and SEM/EDX mapping of O, Al and Co elements.
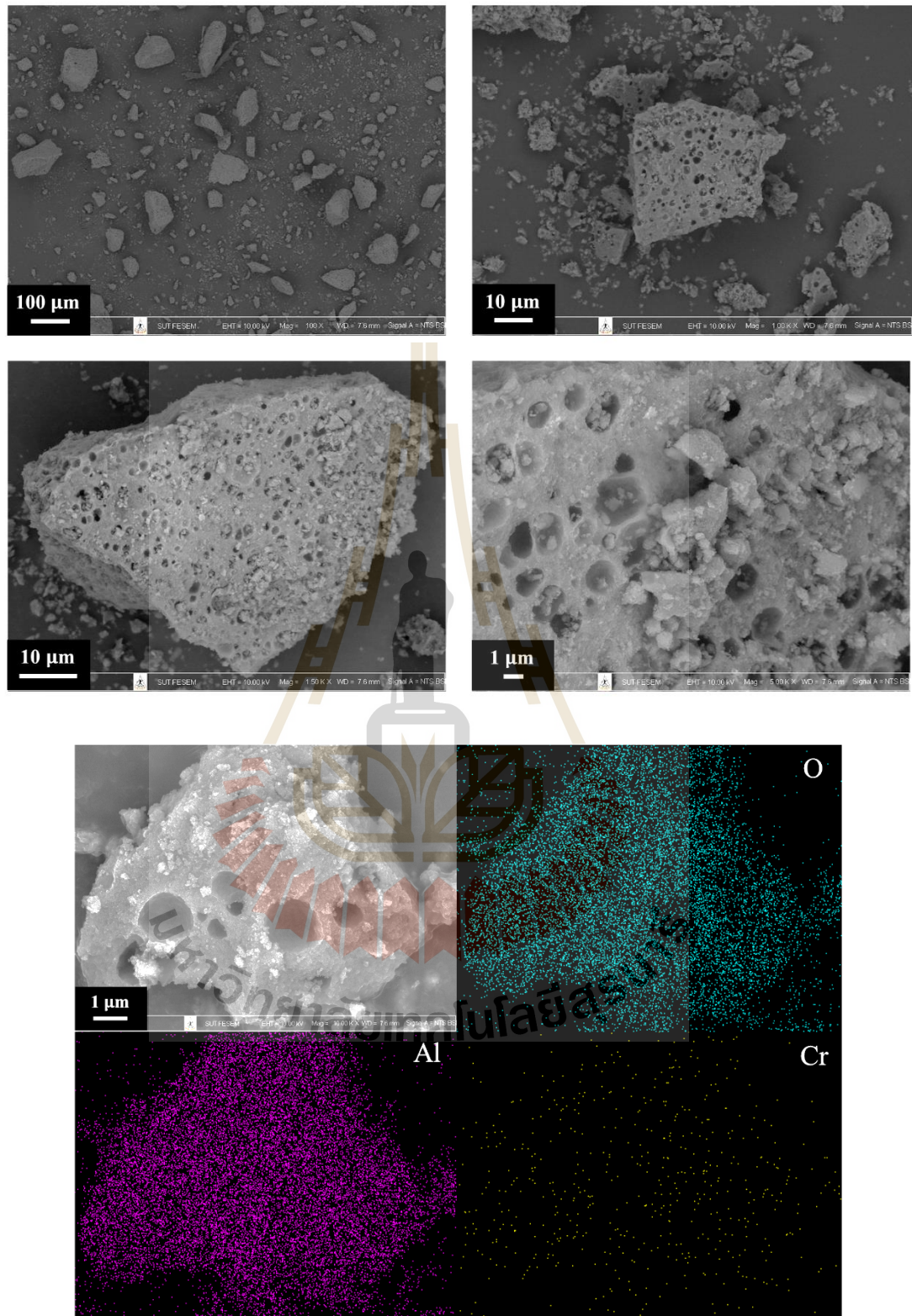
**Figure 4.17** SEM images of Cr/Al$_2$O$_3$ at different magnifications and SEM/EDX mapping of O, Al and Cr elements.
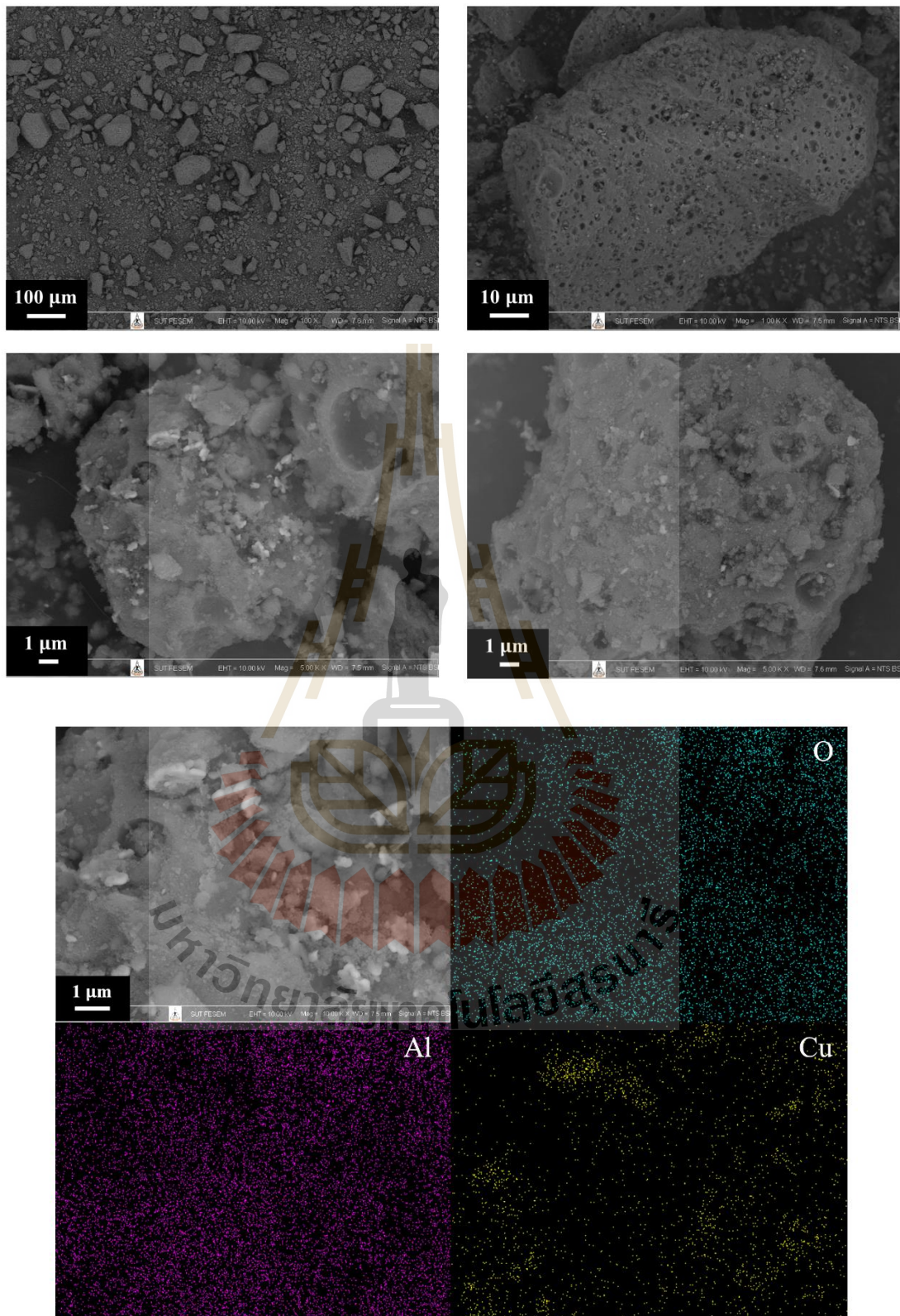
**Figure 4.18** SEM images of Cu/Al$_2$O$_3$ at different magnifications and SEM/EDX mapping of O, Al and Cu elements.
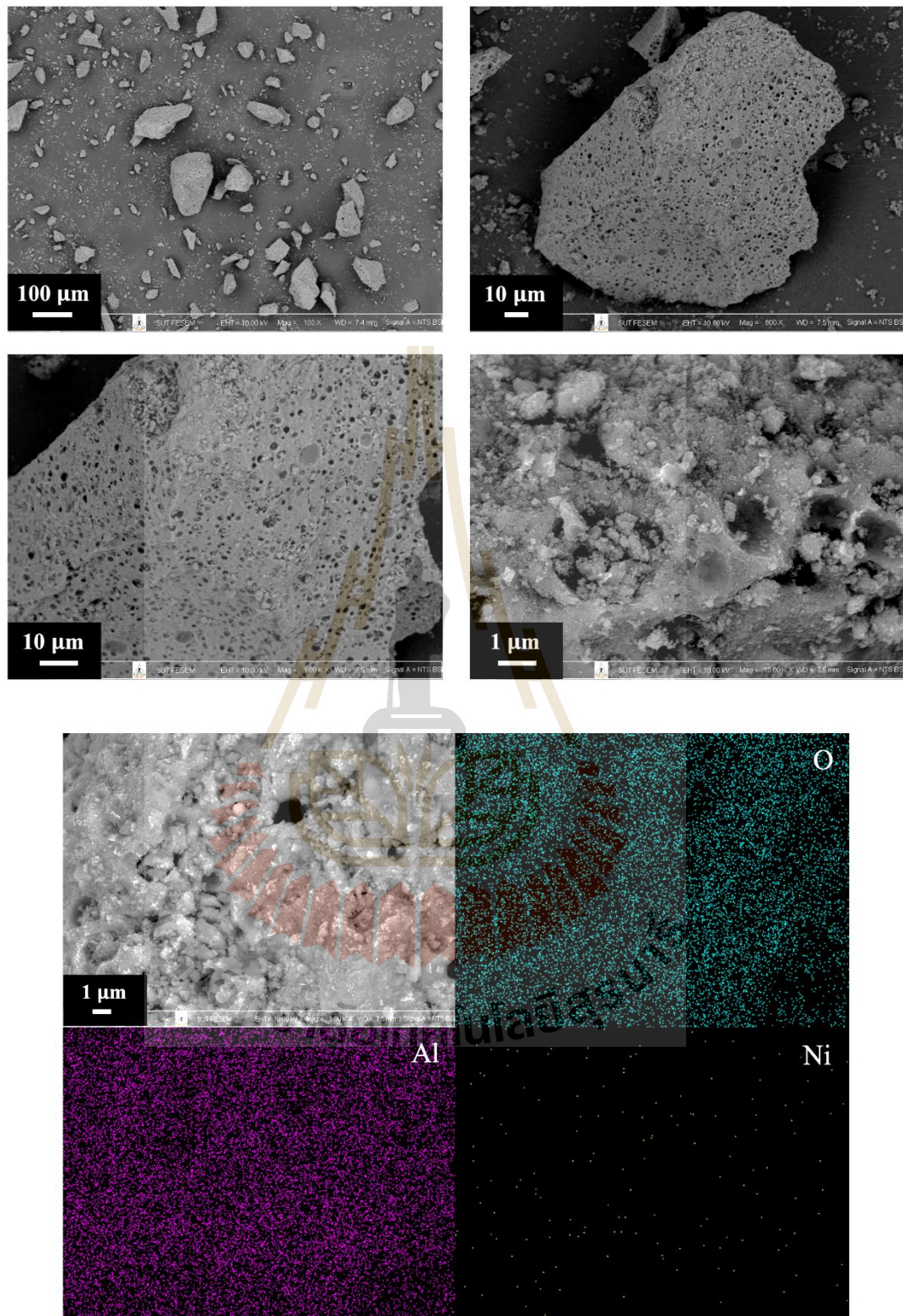
**Figure 4.19** SEM images of Ni/Al₂O₃ at different magnifications and SEM/EDX mapping of O, Al and Ni elements.
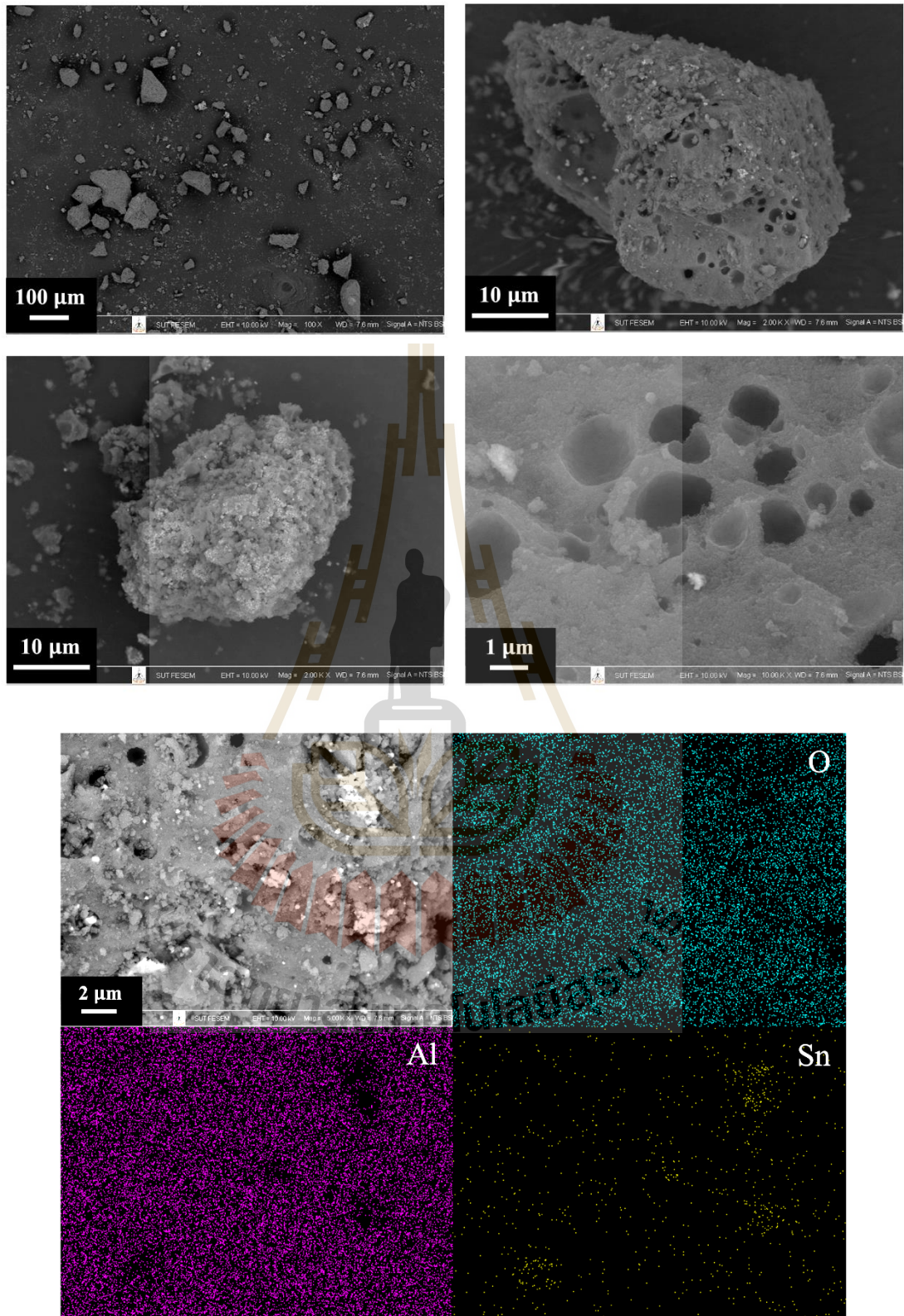
**Figure 4.20** SEM images of Sn/Al₂O₃ at different magnifications and SEM/EDX mapping of O, Al and Sn elements.

### 4.1.5 Transmission electron microscopy (TEM)

TEM images of the $Al_2O_3$ sample (Figure 4.21) investigate the crystallite morphology of $\gamma$-$Al_2O_3$ which contains small size of rod-like particles (Samain et al., 2014). The particles have an average thickness of around 5 nm, which is similar to that calculated from the XRD result. Additionally, the TEM images indicate the interconnection of rod-like particles, which introduce the three dimensional porous structure of $\gamma$-$Al_2O_3$. Moreover, small rod-like particles are observed in the TEM images of the supported metal oxide catalysts, as shown in Figure 4.22-4.26. These can confirm that the crystallite structure of $\gamma$-$Al_2O_3$ is not change after the catalyst preparation. The TEM images of metal supported catalysts are composed of lighter and darker regions. The lighter region is the crystallite phase of the $\gamma$-$Al_2O_3$ support, while the darker region is the crystallite phase of the added metal oxide. The images from all catalysts indicate that the metal oxides do not disperse uniformly on the support.
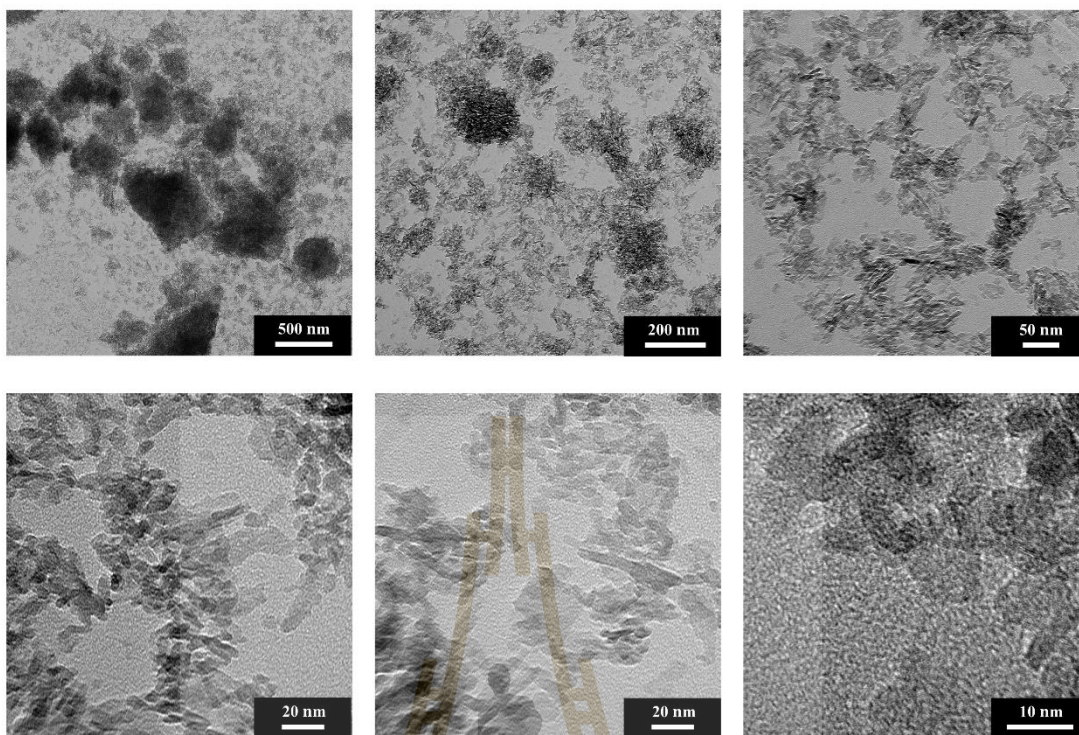
**Figure 4.21** TEM images of $Al_2O_3$ at different magnifications.
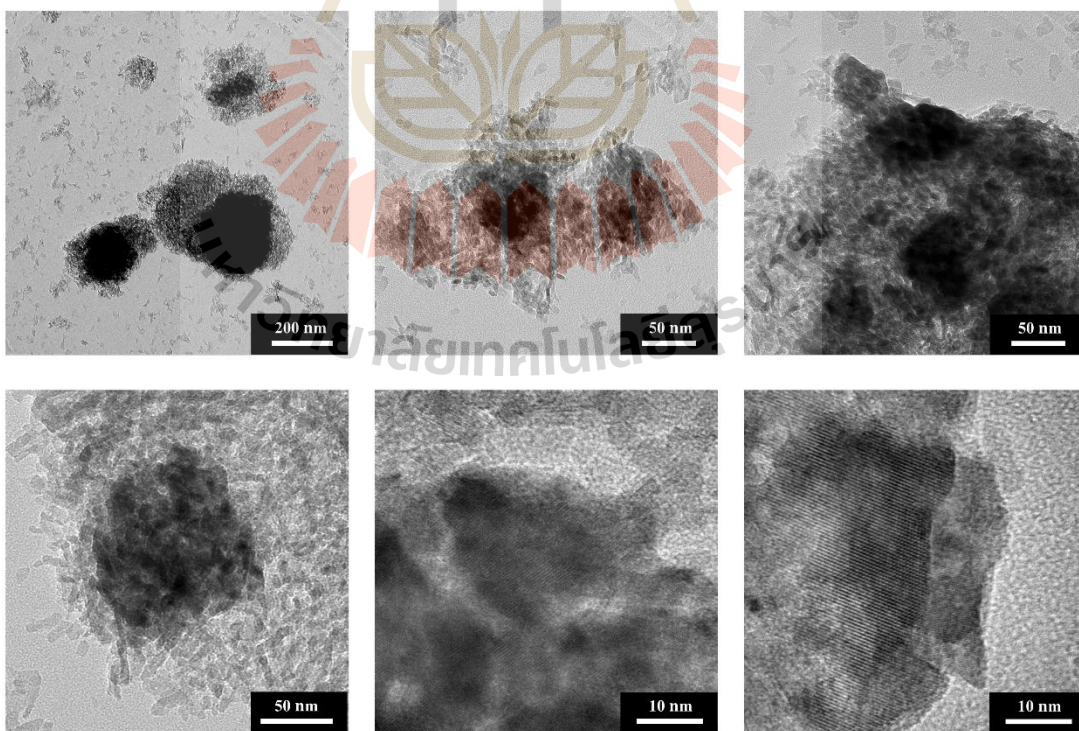


**Figure 4.22** TEM images of $Co/Al_2O_3$ at different magnifications.
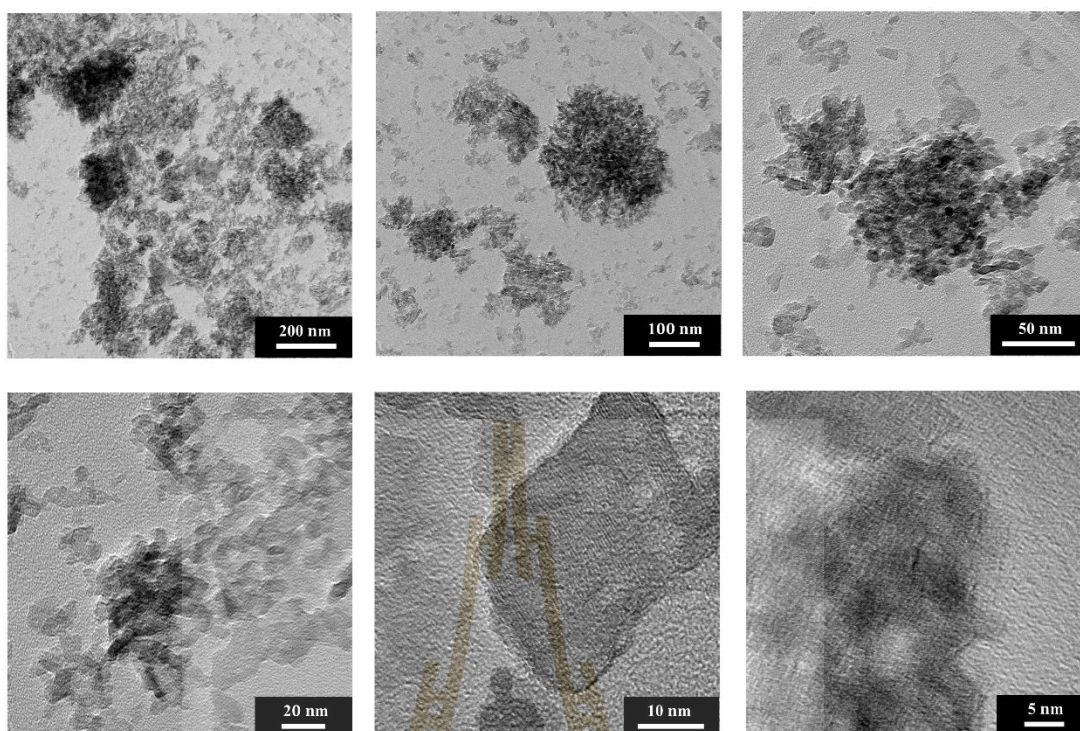
**Figure 4.23** TEM images of Cr/Al$_2$O$_3$ at different magnifications.
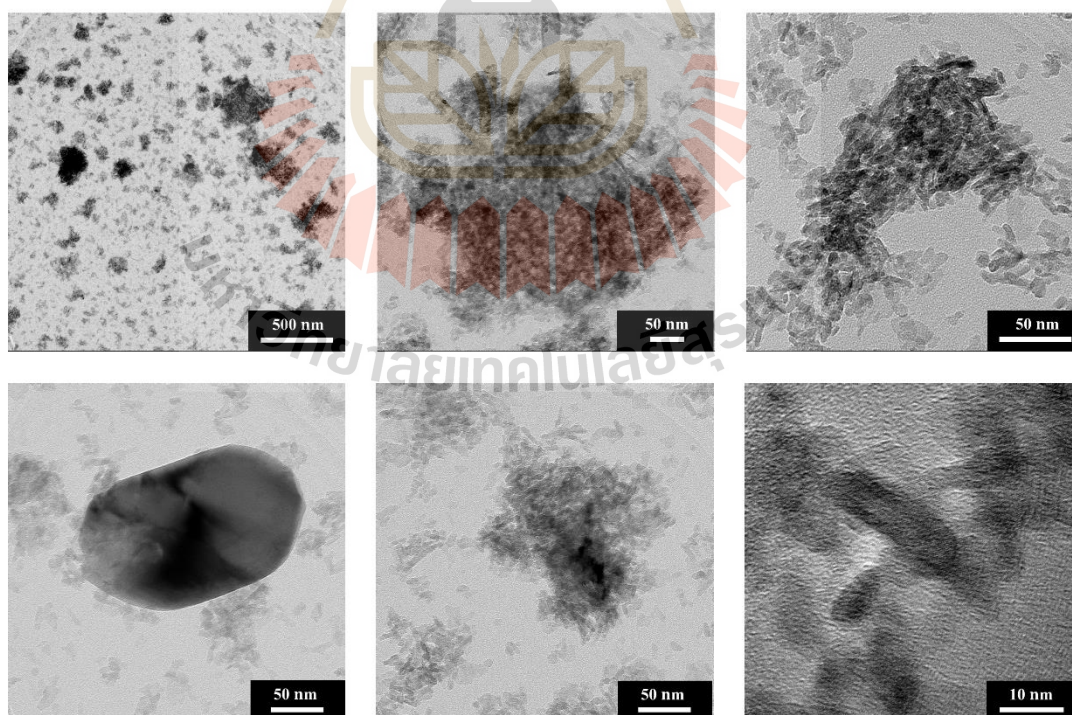


**Figure 4.24** TEM images of Cu/Al$_2$O$_3$ at different magnifications.
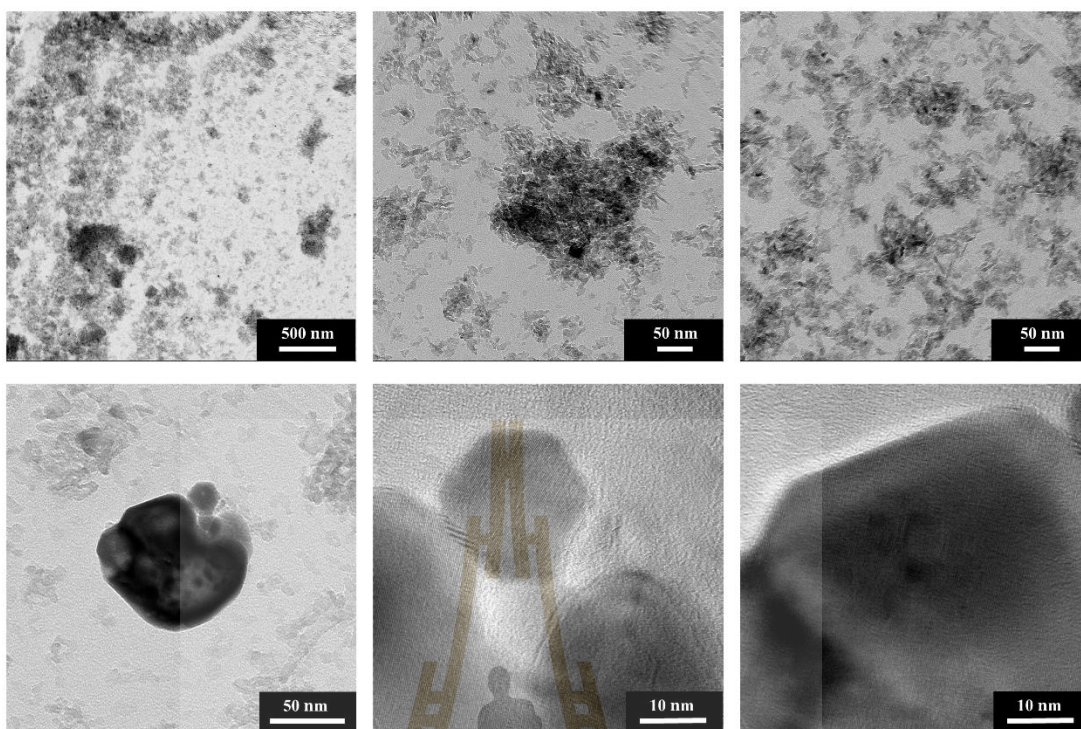
**Figure 4.25** TEM images of Ni/Al$_2$O$_3$ at different magnifications.
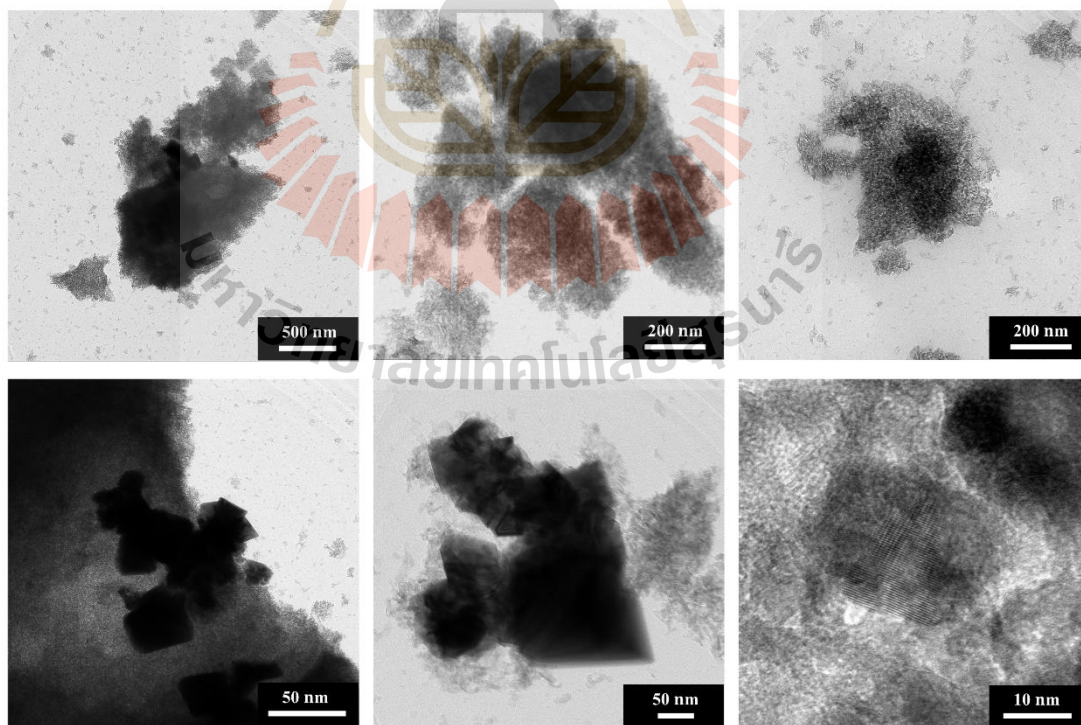


**Figure 4.26** TEM images of Sn/Al$_2$O$_3$ at different magnifications.

### 4.1.6 Temperature-programmed desorption of ammonia (NH$_3$-TPD)

The NH$_3$-TPD profiles of all catalysts are shown in Figure 4.27 and the amount of acid sites in millimole of NH$_3$ per gram of catalyst are summarized in Table 4.8. The NH$_3$-TPD profile of Al$_2$O$_3$ exhibits three desorption peaks at of 178, 350 and 483 °C which relates to weak, medium and strong acid sites, respectively. Those three acid sites correspond to the aluminum atoms with different coordination numbers. Weak and medium acid sites correspond to Al$_{VI}$ center and strong acid site correspond to Al$_{IV}$ center (Gafurov et al., 2015). Meanwhile, the NH$_3$-TPD profiles of supported metal oxide catalysts shows three acid sites with different amount from those of Al$_2$O$_3$. The medium acid site increases whereas the strong acid site decreases. The weak acid site is in the following order: Cr/Al$_2$O$_3$ > Sn/Al$_2$O$_3$ > Cu/Al$_2$O$_3$ > Ni/Al$_2$O$_3$ > Al$_2$O$_3$ > Co/Al$_2$O$_3$. The results suggest that the addition of metal oxides on Al$_2$O$_3$ lead to the increase of weak acid site as well as the decrease of strong acid site. Additionally, Cr/Al$_2$O$_3$ exhibits more amount of weak and medium acid site than other samples. Moreover, the desorption peak of medium acid site shifts to lower temperature.
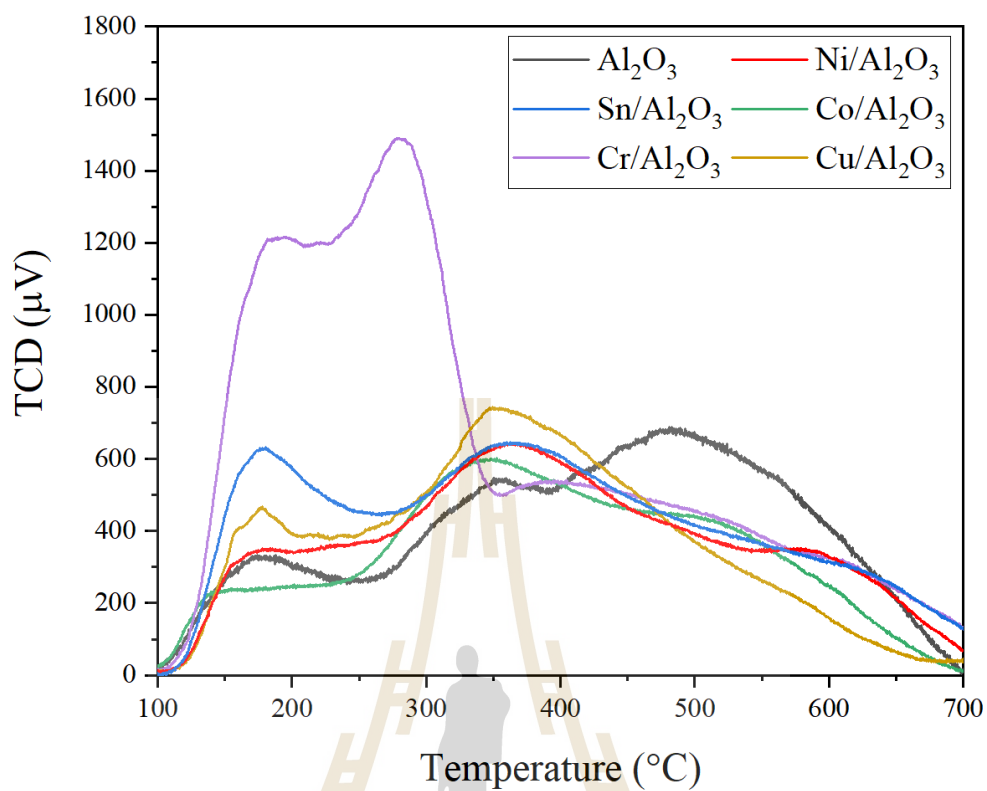
**Figure 4.27** NH$_3$-TPD profiles of Al$_2$O$_3$ and supported catalysts: Co/Al$_2$O$_3$, Cr/Al$_2$O$_3$,

Cu/Al$_2$O$_3$, Ni/Al$_2$O$_3$ and Sn/Al$_2$O$_3$.

**Table 4.8 Summary of amount of acid calculated from NH$_3$-TPD.**

| Sample | Type of acid site | Temperature range (°C) | Peak position (°C) | Peak area (mmol/g) | Total acidity (mmol/g) |
|--------|-------------------|------------------------|--------------------|--------------------|------------------------|
| | | | Amount of acid | | |
| Al$_2$O$_3$ | Weak | 100-250 | 180 | 0.114 | |
| | Medium | 250-400 | 350 | 0.209 | 0.785 |
| | Strong | 400-700 | 490 | 0.462 | |
| Co/Al$_2$O$_3$ | Weak | 100-250 | 180 | 0.104 | |
| | Medium | 250-400 | 350 | 0.249 | 0.639 |
| | Strong | 400-700 | 520 | 0.286 | |
| Cr/Al$_2$O$_3$ | Weak | 100-225 | 180 | 0.302 | |
| | Medium | 225-350 | 280 | 0.478 | 1.164 |
| | Strong | 350-700 | 520 | 0.384 | |
| Cu/Al$_2$O$_3$ | Weak | 100-250 | 180 | 0.138 | |
| | Medium | 250-400 | 350 | 0.282 | 0.678 |
| | Strong | 400-700 | 550 | 0.258 | |
| Ni/Al$_2$O$_3$ | Weak | 100-250 | 180 | 0.124 | |
| | Medium | 250-400 | 370 | 0.258 | 0.706 |
| | Strong | 400-700 | 620 | 0.324 | |
| Sn/Al$_2$O$_3$ | Weak | 100-250 | 180 | 0.187 | |
| | Medium | 250-400 | 370 | 0.259 | 0.730 |
| | Strong | 400-700 | 620 | 0.284 | |

### 4.1.7 Temperature-programmed desorption of carbon dioxide (CO₂-TPD)

The $CO_2$-TPD profiles are shown in Figure 4.28 and the amount of base sites in millimole of $CO_2$ per gram of catalyst calculated from desorbed $CO_2$ are summarized in Table 4.9. All samples displays three desorption peaks relating to interaction between $CO_2$ probe molecule and oxygen anion as base center. They assign to three different basic sites. Weak basic site at 100-200 °C is from bicarbonate species; medium basic site at 200-500 °C is from bidentate carbonate species; and strong basic site at 500-800 °C corresponded to unidentate carbonate species (Fu et al., 1998). The $CO_2$-TPD profiles indicate that the addition of metal oxides changes the basicity from that of $Al_2O_3$ as summarized in Table 4.8.
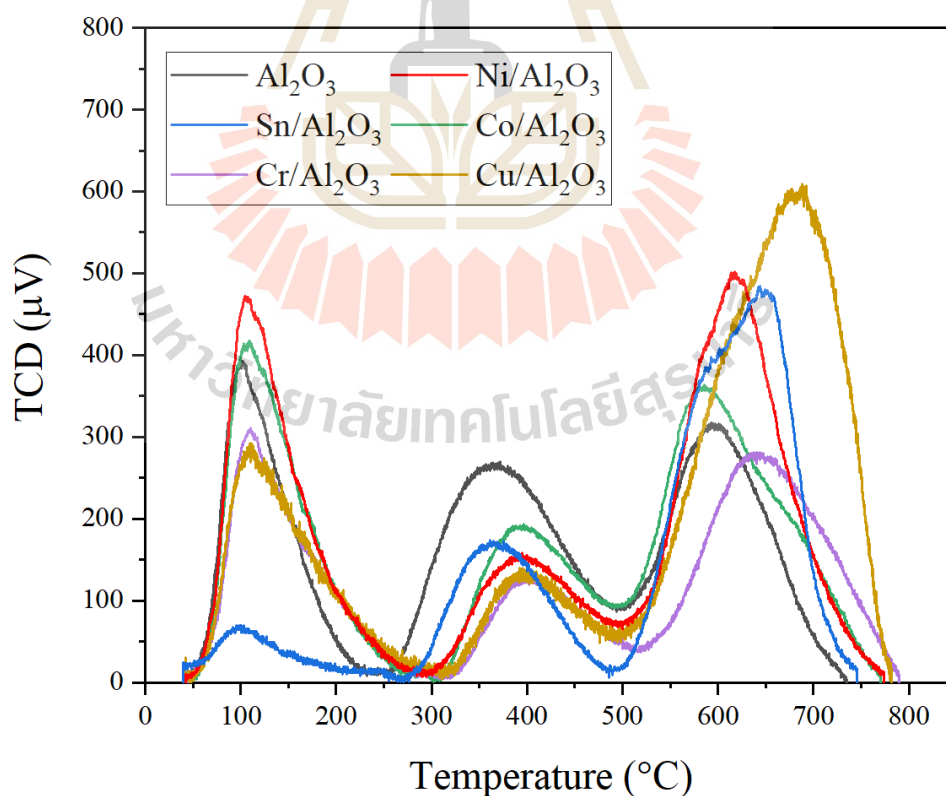


**Figure 4.28** $CO_2$-TPD profiles of $Al_2O_3$ and supported catalysts: $Co/Al_2O_3$, $Cr/Al_2O_3$, $Cu/Al_2O_3$, $Ni/Al_2O_3$ and $Sn/Al_2O_3$.

**Table 4.9 Summary of amount of base calculated from $CO_2$-TPD.**

| Sample | Type of base site | Temperature range (°C) | Peak position (°C) | Peak area (mmol/g) | Total basicity (mmol/g) |
|---|---|---|---|---|---|
| | | | Amount of base | | |
| $Al_2O_3$ | Weak | 100-200 | 110 | 0.065 | |
| | Medium | 250-500 | 360 | 0.080 | 0.217 |
| | Strong | 500-800 | 600 | 0.072 | |
| $Co/Al_2O_3$ | Weak | 100-200 | 110 | 0.073 | |
| | Medium | 250-500 | 400 | 0.048 | 0.228 |
| | Strong | 500-800 | 590 | 0.107 | |
| $Cr/Al_2O_3$ | Weak | 100-200 | 180 | 0.058 | |
| | Medium | 250-500 | 280 | 0.030 | 0.171 |
| | Strong | 500-800 | 645 | 0.083 | |
| $Cu/Al_2O_3$ | Weak | 100-200 | 180 | 0.062 | |
| | Medium | 250-500 | 350 | 0.030 | 0.279 |
| | Strong | 500-800 | 690 | 0.187 | |
| $Ni/Al_2O_3$ | Weak | 100-200 | 180 | 0.085 | |
| | Medium | 250-500 | 370 | 0.040 | 0.252 |
| | Strong | 500-800 | 620 | 0.127 | |
| $Sn/Al_2O_3$ | Weak | 100-200 | 110 | 0.013 | |
| | Medium | 250-500 | 360 | 0.039 | 0.172 |
| | Strong | 500-800 | 650 | 0.120 | |

## 4.2 Catalytic testing results

### 4.2.1 Catalytic screening of various reactants

Figure 4.29 displays conversion of xylose, glucose and glycerol and yield of lactic acid. From xylose as reactant, the xylose conversions are close to 100% and the lactic acid yields are about 20-80%. The lactic acid yields are observed with obviously higher than that from other reactants.

From glucose as reactant, the glucose conversions are close to 100% but the lactic acid yields are below 20%. The results indicate that the transformation of glucose is not selective to lactic acid in the reaction condition used. The glucose could occur dehydration to 5-hydroxymethyl-2-furfural (5-HMF) (Marianou et al., 2018). Otherwise the glucose could lead to fragments of a C4 aldotetrose and a C2 glycolaldehyde through the retro-aldol condensation of aldohexose (Holm et al., 2010). These may result to the low yield of lactic acid produced from glucose.

From glycerol as reactant, the glycerol conversions are below 40% and the lactic acid yields are very low (<1%). The results indicate that the transformation of glycerol is not succeed and the reaction condition used is not selective to lactic acid. The glycerol could be described as a less reactive molecule in this experiment. It consists of hydroxyl group but have no a carbonyl group in the structure which is hard to be transformed under mild reaction conditions. Regarding the literature, the base additive, noble metal and high temperature (200-250 °C) have been applied for lactic acid production from glycerol under hydrothermal conditions (Arcanjo et al., 2017; Ramírez-López et al., 2010; Roy et al., 2011). The base additive could facilitate deprotonated of glycerol. The noble metal has high activity in activating C-H bond

which could help dehydrogenation of glycerol. These indicate that glycerol should be transformed under more extreme conditions than used in this experiment.

All catalysts and this reaction condition are suitable to the conversion of xylose to lactic acid. Therefore, this work is further focused on the catalysis of xylose to lactic acid.
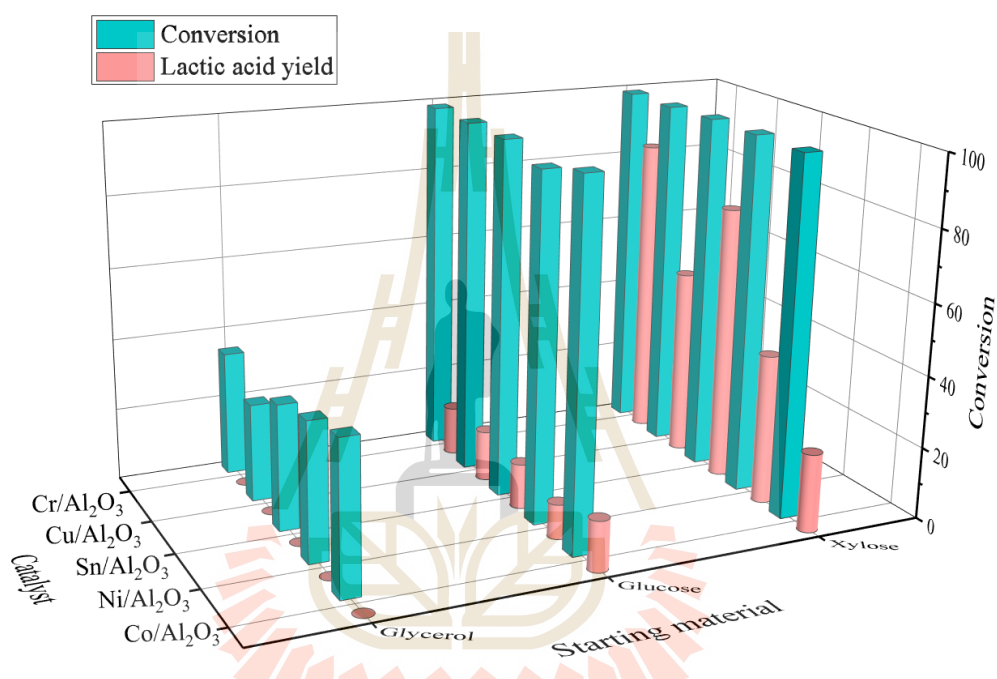


**Figure 4.29** Lactic acid produced from glycerol, glucose and xylose (conditions: 0.5 g catalyst, 170 °C, 15 bar $N_2$, 4 h).

### 4.2.2 Catalytic activities on xylose conversion to lactic acid over several supported metal oxides

Figure 4.30 shows the results of reaction testing on the $Al_2O_3$ support. The conversion of xylose increases with time and becomes constant at the third hour. The product distribution contains lactic acid as a main product and furfural and formic acid as by products.
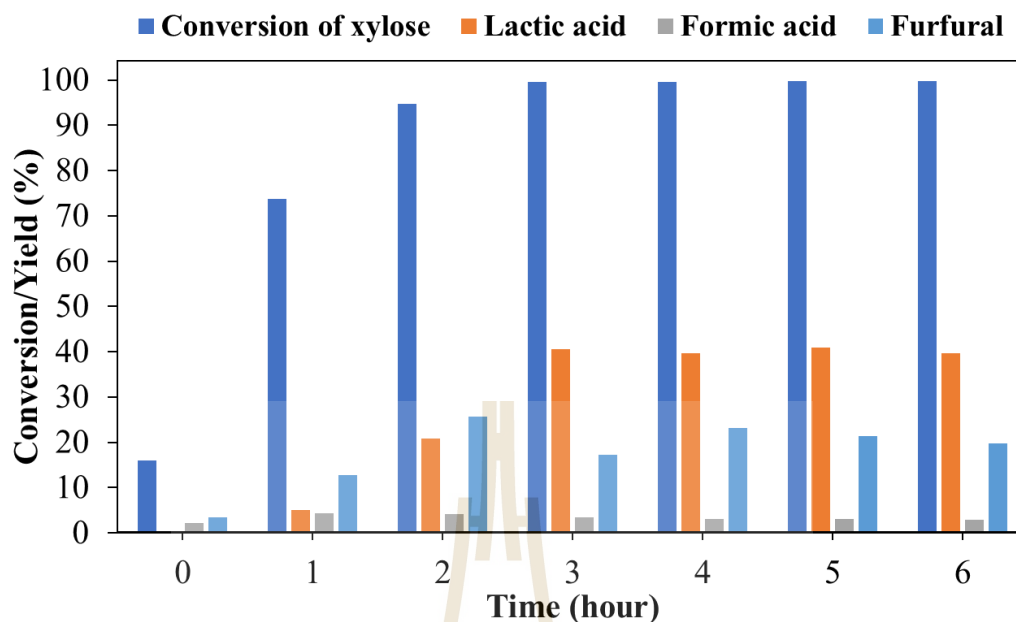
**Figure 4.30** Xylose conversion and product distribution on $Al_2O_3$ (conditions: 0.5 g catalyst, 170 °C, 15 bar $N_2$, 6 h).

All supported catalysts are tested on transformation of xylose at 170 °C for 6 h. The xylose conversions increase with time and are nearly complete (99%) within 4 hours (Figure 4.31). The product distribution from all catalysts is similar to that from $Al_2O_3$. Lactic acid yields from all samples (Figure 4.32) increase with time. The highest yield is observed at fourth hour and the yield becomes constant or decreases after that.

From of all samples, the lactic acid yield increases in the following order: $Cr/Al_2O_3$ (85%) > $Sn/Al_2O_3$ (77%) > $Cu/Al_2O_3$ (52%) > $Ni/Al_2O_3$ (42%) > $Al_2O_3$ (41%) > $Co/Al_2O_3$ (22%). The yields are consistent with the amount of weak acid site of the catalysts. According to Yang et al. (2016), the catalytic performance of Zr-SBA-15 for transformation of xylose to methyl lactate showed the increase of methyl lactate yield with the increase of acidity. It should be noted that amount of weak acidity has influence to the catalytic activities in this reaction condition. The $Cr/Al_2O_3$ which has the highest

weak and medium acid sites provides the best performance. Moreover, chromium oxide has small crystallite size. The small change in basicity was not enough evidenceto differentiate the catalytic results.

The reaction pathways for the transformation of xylose to lactic acid in aqueous solution have been proposed in the literature. First, xylose undergoes retro-aldol condensation w is C-C bond cleavage between C-2 and C-3 carbons to obtain glycoaldehyde (C2) and C3 species. The C3 species could be dihydroxyacetone or glyceradehyde (Holm et al., 2012). However, the glyceraldehyde can be isomerized to the dihydroxyacetone (Xia et al., 2018). It is transformed to 2-hydroxypropenal through dehydration and further to pyruvaldehyde through keto-enol tautomerization. Finally, the pyruvaldehyde undergoes intramolecular Cannizzaro reaction to lactic acid (Yang et al., 2015). The acid sites have been discussed as important role for the key steps. The Lewis acid facilitates retro-aldol condensation of xylose and both Lewis and Brønsted acid have important role for the intramolecular Cannizzaro reaction of pyruvaldehyde to achieve lactic acid selectively (Yang et al., 2015; Yang et al., 2016; Zhang et al., 2018).

However, the catalytic results show that the higher lactic acid yields are obtained from $M/Al_2O_3$ with higher weak acidity compared to bare $Al_2O_3$. This indicates the addition metal oxide of M species of Cr, Sn and Cu can enhance weak acidity which relates to increase lactic acid yield. Apart from that, side products are observed in this work. Furfural can proceeded via dehydration of xylose while formic acid can be formed from decomposition of glycoladehyde (Yang et al., 2015) or from C-C splitting of pyruvaldehyde or glyceraldehyde (Xia et al., 2018) during the transformation of xylose to lactic acid.
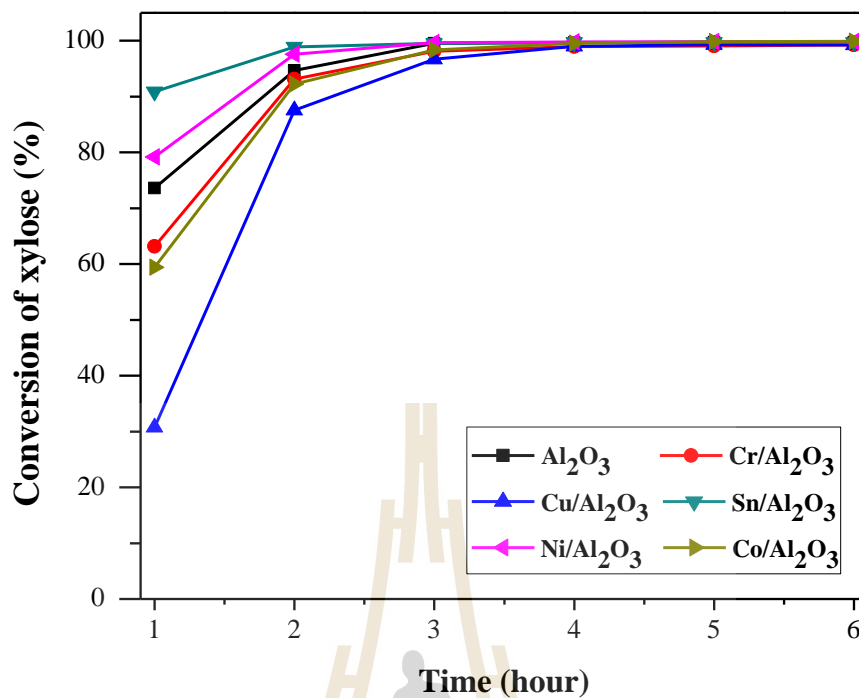
**Figure 4.31** Xylose conversion from all catalysts (condition: 0.5 g catalyst, 170 °C, 15 bar $N_2$, 6 h).
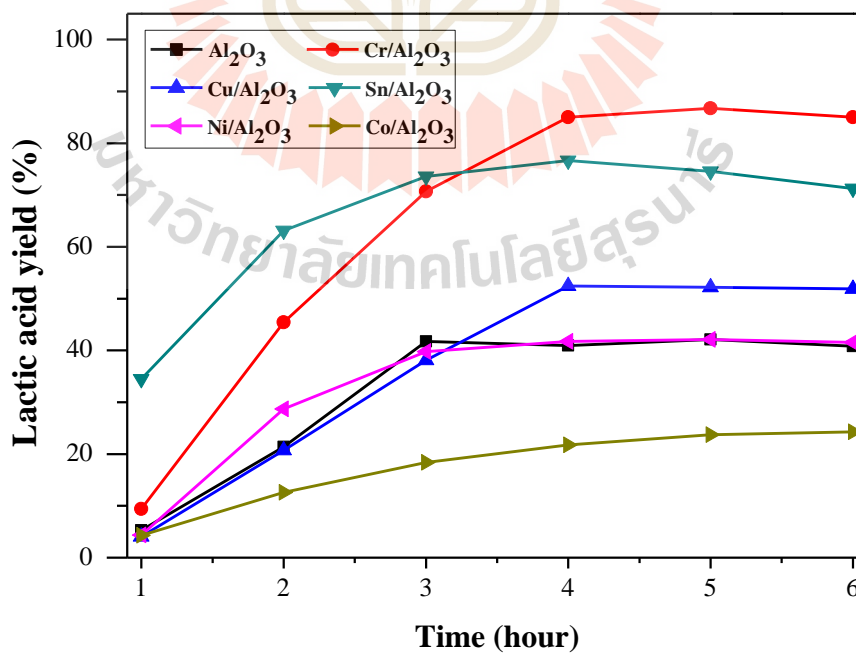


**Figure 4.32** Lactic acid yield from all catalysts (condition: 0.5 g catalyst, 170 °C, 15 bar $N_2$, 6 h).

### 4.2.3 Effect of temperature and catalyst loading over Cr/Al$_2$O$_3$ and Sn/Al$_2$O$_3$

The two best catalysts, Cr/ Al$_2$O$_3$ and Sn/ Al$_2$O$_3$ are investigated under temperature range of 130 to 190 °C at reaction time of 4 hours (Figure 4.33). Those catalysts show xylose conversion approximately 80% at 130 °C and then the conversion increases with temperature to 99% at 170 °C and becomes constant at a higher temperature of 190 °C. The lactic acid as a main product and furfural as a by product. Those catalysts show lactic acid yield increases with the temperature and the highest yield is obtained at 170 °C. However, the yield from both catalysts decreases at 190 °C may because lactic acid further transforms to other small organic acids (Srokol et al., 2004). Otherwise, the small organic acids could be produced from C-C splitting of pyruvaldehyde or glyceraldehyde which are intermediates in this reaction (Xia et al., 2018).

Furthermore, Cr/Al$_2$O$_3$ and Sn/Al$_2$O$_3$ are investigated the amount of catalyst required in a reaction batch. The results from both catalyst are similar (Figure 4.34). The conversion is nearly completed from the use of all catalyst loading in this experiment. The lactic acid yield increases with catalyst loading which could has more active site. The results from the use of 0. 5 and 1. 0 g catalyst are similar. Thus, 0. 5 g catalyst is enough for the batch reactor 75 ml.
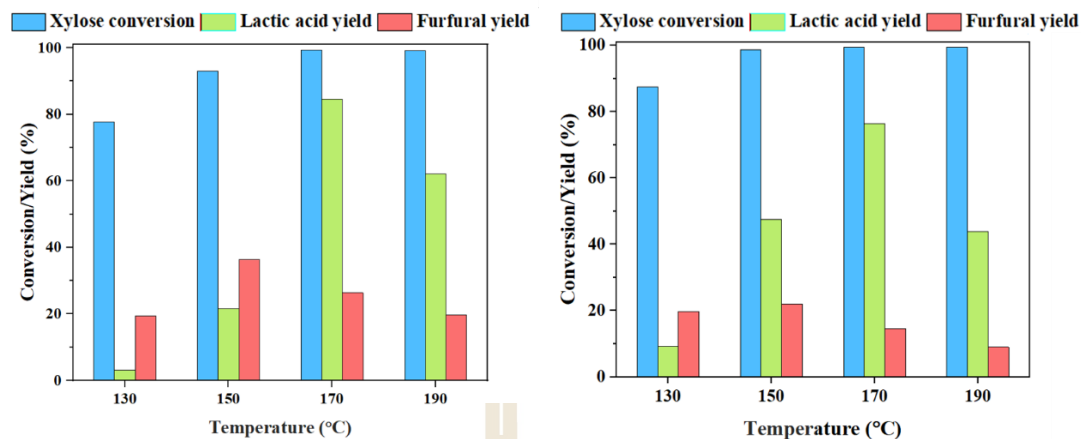
**Figure 4.33** Xylose conversion and lactic acid yield under various temperatures of Cr/Al$_2$O$_3$ (left) and Sn/Al$_2$O$_3$ (right), (condition: 0.5 g catalyst, 15 bar N$_2$, 4 h).
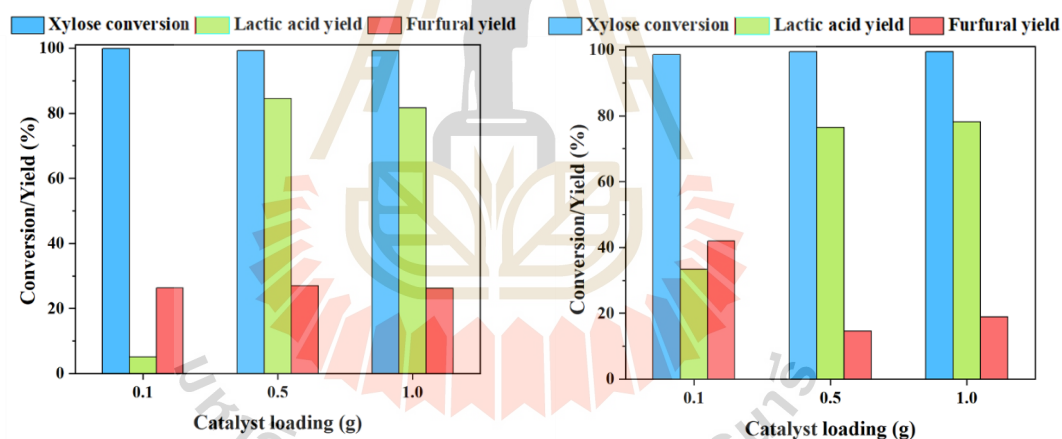


**Figure 4.34** Xylose conversion and lactic acid yield under various catalyst loading of Cr/Al$_2$O$_3$ (left) and Sn/Al$_2$O$_3$ (right), (condition: 170 °C, 15 bar N$_2$, 4 h).

## 4.3 References

Akhavan, O., Azimirad, R., Safa, S., and Hasani, E. (2011). CuO/Cu(OH)$_2$ hierarchical nanostructures as bactericidal photocatalysts. **Journal of Materials Chemistry**. 21(26): 9634-9640.

Arcanjo, M. R. A., Silva, I. J., Rodríguez-Castellón, E., Infantes-Molina, A., and Vieira, R. S. (2017). Conversion of glycerol into lactic acid using Pd or Pt supported on carbon as catalyst. **Catalysis Today**. 279: 317-326.

Fu, Y., Zhang, L., Yue, B., Chen, X., and He, H. (2018). Simultaneous characterization of solid acidity and basicity of metal oxide catalysts via the solid-state NMR technique. **The Journal of Physical Chemistry C**. 122(42): 24094-24102.

Gafurov, M. R., Mukhambetov, I. N., Yavkin, B. V., Mamin, G. V., Lamberov, A. A., and Orlinskii, S. B. (2015). Quantitative analysis of Lewis acid centers of γ-alumina by using EPR of the adsorbed anthraquinone as a probe molecule: comparison with the pyridine, carbon monoxide IR, and TPD of ammonia. **Journal of Physical Chemistry C**. 119(49): 27410-27415.

Holm, Martin S., Pagán-Torres, Y. J., Saravanamurugan, S., Riisager, A., Dumesic, J. A., and Taarning, E. (2012). Sn-Beta catalysed conversion of hemicellulosic sugars. **Green Chemistry**. 14(3): 702-706.

Holm, Martin Spangsberg, Saravanamurugan, S., and Taarning, E. (2010). Conversion of sugars to lactic acid derivatives using heterogeneous zeotype catalysts. **Science**. 328(5978): 602-605.

Li, C. Y., Zhang, H. J., and Chen, Z. Q. (2013). Reaction between NiO and $Al_2O_3$ in NiO/γ-$Al_2O_3$ catalysts probed by positronium atom. **Applied Surface Science**. 266: 17-21.

Marianou, A. A., Michailof, C. M., Pineda, A., Iliopoulou, E. F., Triantafyllidis, K. S., and Lappas, A. A. (2018). Effect of Lewis and Brønsted acidity on glucose conversion to 5-HMF and lactic acid in aqueous and organic media. **Applied Catalysis A: General**. 555(2010): 75-87.

Ramírez-López, C. A., Ochoa-Gómez, J. R., Fernández-Santos, M., Gómez-Jiménez-Aberasturi, O., Alonso-Vicario, A., and Torrecilla-Soria, J. (2010). Synthesis of lactic acid by alkaline hydrothermal conversion of glycerol at high glycerol concentration. **Industrial and Engineering Chemistry Research**. 49(14): 6270-6278.

Roy, D., Subramaniam, B., and Chaudhari, R. V. (2011). Cu-based catalysts show low temperature activity for glycerol conversion to lactic acid. **ACS Catalysis**. 1(5): 548-551.

Samain, L., Häussermann, U., Jaworski, A., Edén, M., Ladd, D. M., and Seo, D.-K. (2014). Structural analysis of highly porous $\gamma$-Al$_2$O$_3$. **Journal of Solid State Chemistry**. 217: 1-8.

Srokol, Z., Estrik, A. Van, Strik, R. C. J., Maschmeyer, T., and Peters, J. A. (2004). Hydrothermal upgrading of biomass to biofuel; studies on some monosaccharide model compounds. **Carbohydrate Research**. 339(10): 1717-1726.

Strohmeier, B. R. (1994). Gamma-alumina ($\gamma$-Al$_2$O$_3$) by XPS. **Surface Science Spectra**. 3(2): 135-140.

Süzer, Ş., Voscoboinikov, T., Hallam, K. R., and Allen, G. C. (1996). Electron spectroscopic investigation of Sn coatings on glasses. **Fresenius' Journal of Analytical Chemistry**. 355(5-6): 654-656.

Thommes, M., Kaneko, K., Neimark, A. V., Thommes, M., Sing, K. S. W., Rodriguez-Reinoso, F., Olivier, J. P., Kaneko, K., and Rouquerol, J. (2015). Physisorption of gases, with special reference to the evaluation of surface area and pore size distribution (IUPAC Technical Report). **Pure and Applied Chemistry**. 87(9-10): 1051-1069.

Wang, Y., Yang, J., Gu, R., Peng, L., Guo, X., Xue, N., Zhu, Y., and Ding, W. (2018). Crystal-facet effect of γ-Al$_2$O$_3$ on supporting CrO$_x$ for catalytic semihydrogenation of acetylene. **ACS Catalysis**. 8(7): 6419-6425.

Xia, M., Dong, W., Gu, M., Chang, C., Shen, Z., and Zhang, Y. (2018). Zeolite for lactic acid synthesis from biomass-derived carbohydrates. **RSC Advances**. 8: 8965-8975.

Xu, M., Iglesia, E., Apestegu, C. R., Cosimo, D. I., and Al, E. T. (1998). Structure and surface and catalytic properties of Mg-Al basic oxides. **Journal of Catalysis**. 178(2): 499-510.

Yang, L., Su, J., Carl, S., Lynam, J. G., Yang, X., and Lin, H. (2015). Catalytic conversion of hemicellulosic biomass to lactic acid in pH neutral aqueous phase media. **Applied Catalysis B: Environmental**. 162: 149-157.

Yang, L., Yang, X., Tian, E., Vattipalli, V., Fan, W., and Lin, H. (2016). Mechanistic insights into the production of methyl lactate by catalytic conversion of carbohydrates on mesoporous Zr-SBA-15. **Journal of Catalysis**. 333: 207-216.

Yang, X., Chen, J., Chen, Y., Feng, P., Lai, H., Li, J., and Luo, X. (2018). Novel Co$_3$O$_4$ nanoparticles/nitrogen-doped carbon composites with extraordinary catalytic activity for oxygen evolution reaction (OER). **Nano-Micro Letters**. 10(15): 1-11.

Zhang, H., Hu, Y., Qi, L., He, J., Li, H., and Yang, S. (2018). Chemocatalytic production of lactates from biomass-derived sugars. **International Journal of Chemical Engineering**. 2018(7617685): 1-18.

Zhou, J., Guo, L., Guo, X., Mao, J., and Zhang, S. (2010). Selective hydrogenolysis of glycerol to propanediols on supported Cu-containing bimetallic catalysts. **Green Chemistry**. 12(10): 1835-1843.

# CHAPTER V

# CONCLUSIONS

Heterogeneous catalysts consisting of metal oxides supported on $\gamma$-$Al_2O_3$ including $Co/Al_2O_3$, $Cr/Al_2O_3$, $Cu/Al_2O_3$, $Ni/Al_2O_3$, and $Sn/Al_2O_3$ are prepared by impregnation method. All catalysts and the $Al_2O_3$ support are analyzed by several techniques. XRD confirms the phase of metal oxides ($\gamma$-$Al_2O_3$, $CuO$, $Co_3O_4$, $NiO$, $NiAl_2O_4$, and $SnO_2$) from all catalysts except $Cr/Al_2O_3$. The phase of chromium oxide is not observed implying that it had amorphous phase and/or good dispersion. XPS and XANES confirm the oxidation state and elemental composition of each metal species. The existence of $Cr^{3+}$ and $Cr^{6+}$ species on the $Cr/Al_2O_3$ catalyst is confirmed. $N_2$ adsorption-desorption analysis reveals that all catalysts have both micropores and mesopores with similar surface area. SEM and TEM images of all catalysts show similar morphology. Moreover, $NH_3$-TPD results lead to a conclusion that the catalyst acidity is different from the $Al_2O_3$ support, namely, they have more medium acid sites but less strong acid sites. The weak acid sites increase in the following order: $Cr/Al_2O_3$ > $Sn/Al_2O_3$ > $Cu/Al_2O_3$ > $Ni/Al_2O_3$ > $Al_2O_3$ > $Co/Al_2O_3$. Meanwhile, $CO_2$-TPD shows that the catalyst basicity slightly changes from $Al_2O_3$. All catalysts including the $Al_2O_3$ support are tested on the lactic acid production from xylose, glucose, and glycerol. The testing is carried out in a batch reactor 75 ml under an aqueous solution and pressure 15 bar $N_2$. The highest conversion and lactic acid yield are obtained from xylose. Glucose produces more side products and glycerol requires more extreme

reaction condition. The xylose is further tested under 6 h. The conversion and lactic acid yield increase with time. The lactic acid yield relates to the amount of weak acid sites and increases in the following order: $Cr/Al_2O_3$ (85%) > $Sn/Al_2O_3$ (77%) > $Cu/Al_2O_3$ (52%) > $Ni/Al_2O_3$ (42%) > $Al_2O_3$ (41%) > $Co/Al_2O_3$ (22%). The $Cr/Al_2O_3$ is the best catalyst due to the highest number of weak and medium acid sites. The optimal temperature and catalyst loading of $Cr/Al_2O_3$ are 170 °C and 0.5 g, respectively.

# CURRICULUM VITAE

# Chanokporn Kosri

**Address**          149 No. 3, Khokkhamin Sub-district, Plabplachai District,

Buriram, Thailand, 31250 Email: kosri.c@hotmail.com

**Education**

2017                   B. Sc. (Chemistry) with honors

Suranaree University of Technology (SUT), Nakhon

Ratchasima, Thailand

2017- 2019        Student in M. Sc. program in Chemistry, SUT

**Scholarship**

2013-Present     Development and Promotion of Science and Technology

Talents Project (DPST)

**Publications**

**Kosri, C.**, Deekamwong, K., Sophiphun, O., Osakoo, N., Chanlek, N., Föttinger, K.,
and Wittayakun, J. (2017) Comparison of Fe/HBEA catalysts from incipient wetness
impregnation with various loading on phenol hydroxylation. **Reaction Kinetics,
Mechanisms and Catalysis**. 121(2): 751-761.

**Kosri, C.**, Sirapassorn Kiatphuengporn, S., Butburee, T., Youngjan, S., Tongrutkaew,
S., Fuangnawakij, K., Chanlek, N., Kijkhuntod, P., Wittayakun, J., and Khemthong, P.
(2019) Selective conversion of xylose to lactic acid over metal oxides supported on
$Al_2O_3$ catalysts (submitted)